Quaternized fluorene-based hydroxide exchange membranes and polymers: design, synthesis, and characterization

Allushi, Andrit

2022

Quaternized fluorene-based hydroxide exchange membranes and polymers: design, synthesis, and characterization

ANDRIT ALLUSHI | CENTRE FOR ANALYSIS AND SYNTHESIS | LUND UNIVERSITY

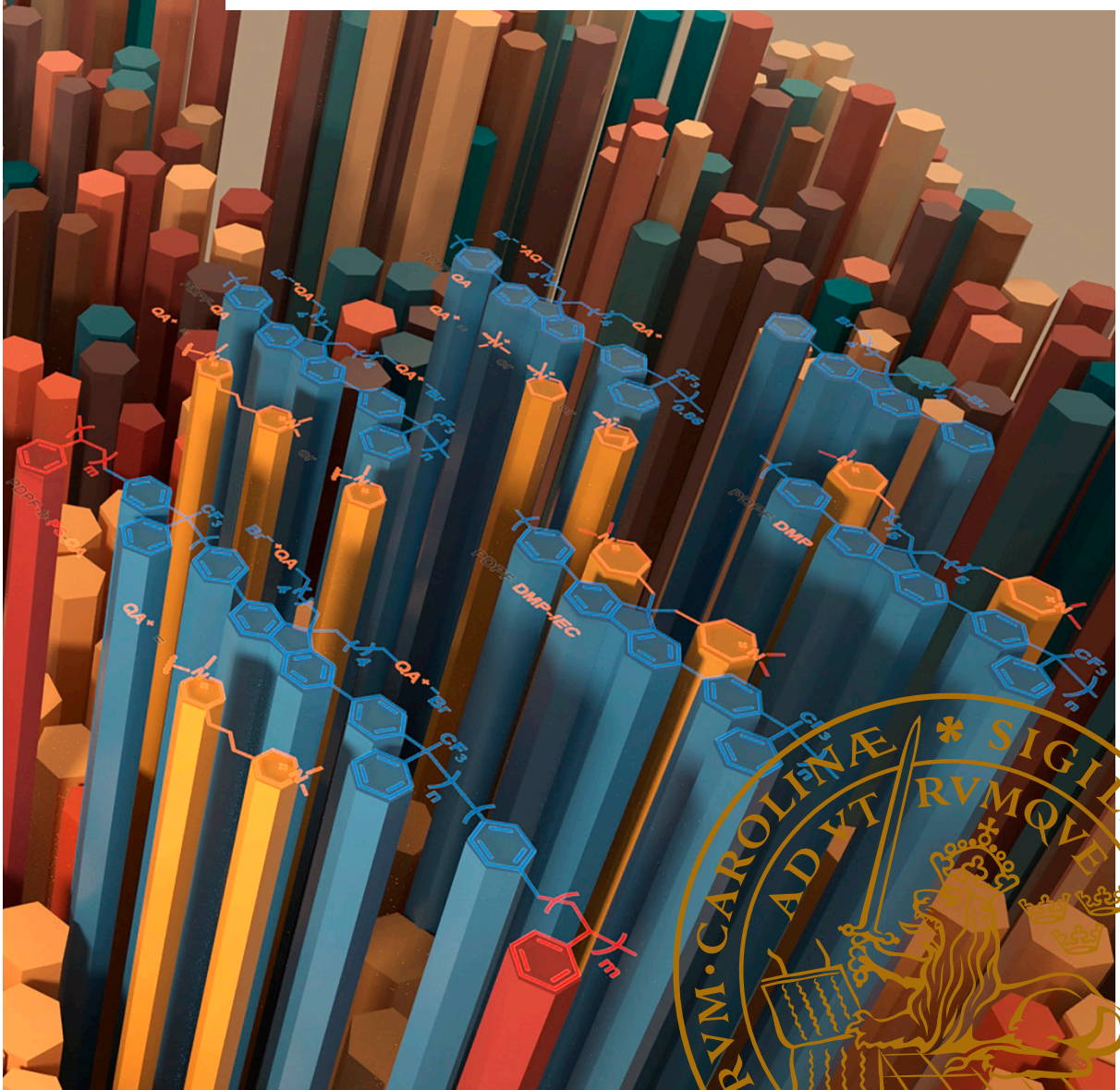

Quaternized fluorene-based hydroxide exchange membranes and polymers: design, synthesis, and characterization

Quaternized fluorene-based hydroxide exchange membranes and polymers: design, synthesis, and characterization

Andrit Allushi

LUND
UNIVERSITY

DOCTORAL DISSERTATION

by due permission of the Faculty of Engineering, Lund University, Sweden.
To be defended at Kemicentrum , Lecture Hall K:A on November 10, at 09:00.

Faculty opponent
Dr. Jochen Meier-Haack,
Leibnitz Institute of Polymer Research Dresden

Organization LUND UNIVERSITY	**Document name** Doctoral Dissertation
	Date of issue 2022.11.10
Author(s) Andrit Allushi	Sponsoring organization

Title and subtitle

Quaternized fluorene-based hydroxide exchange membranes and polymers: design, synthesis, and characterization

In modern society, the consumption of fossil fuels has been increasing drastically, leading to significant emissions of carbon dioxide (CO_2), air pollution, global warming, and political and economic imbalances. This has increased the interest in renewable and sustainable energy sources such as wind- and hydropower, solar energy, and in energy conversion by fuel cell technology, and water electrolyses. Fuel cell technology is considered attractive because it can be applied not only in stationary applications such as power generation systems, but also in automotive applications. The fuel cell converts chemical energy into electricity with only water as a by-product. Anion exchange membrane fuel cells (AEMFCs) operate under basic conditions. They are undoubtedly considered the next generation fuel cell technology devices, due to their distinct advantages, for example, possibility to use non-noble metals as a catalysts for electrochemical reactions, faster oxygen reduction kinetics as well as flexibility in the fuel. Anion exchange membrane (AEM) is the core component in this fuel cell because it is responsible for the hydroxide transportation from cathode to anode electrolyte and it has a direct impact on the fuel cell performance and durability. The AEM consist of a solid polymer backbone, cationic groups tethered covalently to it, and hydroxide ions (OH^-) as counter ions. During long-term operation of the fuel cell, the AEM is prone to be attacked, resulting in degradation of the ion conductivity and efficiency of the cell. Therefore, the requirements for AEMs to be considered are high ion conductivity, excellent alkaline stability, and low cost. To reach these targets, novel and different polymer architectures have been to be synthesized and investigated.

In the current work, ether-free polymer backbone structures functionalized with N-heterocyclic ammonium groups (NHAs) were synthesized and characterized as candidate membranes for fuel cell applications. Polymer backbone architectures were based on fluorene units, which were tethered with mono- and spirocyclic quaternary ammonium groups via an alkyl spacer. Different synthetic methods, including alkylations and Suzuki coupling, were used for the monomer synthesis. Acid-mediated polyhydroxyalkylation reactions and atom transfer radical polymerizations (ATRPs) were employed to synthesize polymer backbones with unique architectures. The introduction of the cationic quaternary ammonium (QA) groups was achieved by Menshutkin reactions. The membranes were characterized with regard to hydroxide conductivity, water uptake, morphology, and thermal and alkaline stability. The effects of both the polymer backbone structure and the QA structure, and the position at which the QA group is attached to the polymer backbone, have been investigated with respect to the properties mentioned above.

Key words: anion exchange membrane, fuel cell, quaternary ammonium, alkaline stability, N-heterocyclic ammonium

Classification system and/or index terms (if any)

Supplementary bibliographical information		**Language** English
ISSN and key title		**ISBN:** 978-91-7422-902-8(Print) **ISBN:** 978-91-7422-903-5(Digital)
Recipient's notes	**Number of pages** 230	Price
	Security classification	

Signature 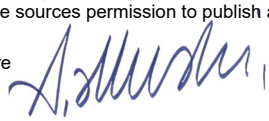 Date 2022-10-04

Quaternized fluorene-based hydroxide exchange membranes and polymers: design, synthesis, and characterization

Andrit Allushi

LUND
UNIVERSITY

Coverimage by Besmir Kamberi

Faculty of Engineering, Department of Chemistry, CAS
Lund University

ISBN 978-91-7422-902-8 (Print)
ISBN: 978-91-7422-903-5 (Digital)

Printed in Sweden by Media-Tryck, Lund University
Lund 2022

The things you think about
determine the quality of your mind

Marcus Aurelius

Abstract

In modern society, the consumption of fossil fuels has been increasing drastically, leading to significant emissions of carbon dioxide (CO_2), air pollution, global warming, and political and economic imbalances. This has increased the interest in renewable and sustainable energy sources such as wind- and hydropower, solar energy, and in energy conversion by fuel cell technology, and water electrolyses. Fuel cell technology is considered attractive because it can be applied not only in stationary applications such as power generation systems but also in automotive applications. The fuel cell converts chemical energy into electricity with only water as a by-product. Anion exchange membrane fuel cells (AEMFCs) operate under basic conditions. They are undoubtedly considered the next generation fuel cell technology devices, due to their distinct advantages, for example, possibility to use non-noble metals as a catalysts for electrochemical reactions, faster oxygen reduction kinetics as well as flexibility in the fuel. Anion exchange membrane (AEM) is the core component in this fuel cell because it is responsible for the hydroxide transportation from cathode to anode electrolyte and it has a direct impact on the fuel cell performance and durability. The AEM consist of a solid polymer backbone, cationic groups tethered covalently to it, and hydroxide ions (OH^-) as counter ions. During long-term operation of the fuel cell, the AEM is prone to be attacked, resulting in degradation of the ion conductivity and efficiency of the cell. Therefore, the requirements for AEMs to be considered are high ion conductivity, excellent alkaline stability, and low cost. To reach these targets, novel and different polymer architectures have been to be synthesized and investigated.

In the current work, ether-free polymer backbone structures functionalized with N-heterocyclic ammonium groups (NHAs) were synthesized and characterized as candidate membranes for fuel cell applications. Polymer backbone architectures were based on fluorene units, which were tethered with mono- and spirocyclic quaternary ammonium groups via an alkyl spacer. Different synthetic methods, including alkylations and Suzuki coupling, were used for the monomer synthesis. Acid-mediated polyhydroxyalkylation reactions and atom transfer radical polymerizations (ATRPs) were employed to synthesize polymer backbones with unique architectures. The introduction of the cationic quaternary ammonium (QA) groups was achieved by Menshutkin reactions. The membranes were characterized with regard to hydroxide conductivity, water uptake, morphology,

and thermal and alkaline stability. The effects of both the polymer backbone structure and the QA structure, and the position at which the QA group is attached to the polymer backbone, have been investigated with respect to the properties mentioned above.

List of Appended Papers

This thesis is based on the papers listed below.

I. **Ether-free polyfluorenes tethered with quinuclidinium cations as hydroxide exchange membranes**
Andrit Allushi, Thanh Huong Pham, Joel S. Olsson and Patric Jannasch
Journal of Materials Chemistry A, **2019***,* 7, 27164-27174

II. **Highly conductive hydroxide exchange membranes containing fluorene-units tethered with dual pairs of quaternary piperidinium cations**
Andrit Allushi, Thanh Huong Pham and Patric Jannasch
Journal Membrane Science, **2021**, 632, 119376-119386.

III. **Hydroxide conducting BAB triblock copolymers with a central polyfluorene block densely tethered with 1,1-dimethylpiperidinium cations**
Andrit Allushi, Pegah Mansouri Bakvand and Patric Jannasch
In manuscript

IV. **Rational Molecular Design of Anion Exchange Membranes Functionalized with Alicyclic Quaternary Ammonium Cations**
Thanh Huong Pham, Andrit Allushi, Joel S. Olsson and Patric Jannasch
Polymer Chemistry, **2020, 11,** 6953-6963

V. **Polyfluorenes bearing 1,1-dimethylpiperidinium cations on short spacers for durable anion exchange membranes.**
Andrit Allushi, Pegah Mansouri Bakvand and Patric Jannasch
Submitted

My contribution to the publications.

I. I planned and performed all the experimental work. I wrote the first draft of the paper.

II. I planned and performed all the experimental work. I wrote the first draft of the paper

III. I planned and performed all the experimental work. I wrote the first draft of the paper.

IV. I performed some laboratory work. I contributed on the planning of the project, and analysing/interpreting the result. I prepared the first draft of the paper.

V. I performed some laboratory work. I took an active plane in planning the project, analysing the result and writing the article.

Abbreviations

AEM	anion exchange membrane
PAA	poly(arylene alkylene)
HEM	hydroxide exchange membrane
AEMFC	anion exchange membrane fuel cell
PEMFC	proton exchange membrane fuel cell
AEMWE	anion exchange membrane water electrolysis
FC	fuel cell
IEC	ion- exchange capacity (meq.g-1 or mmol g-1)
MEA	membrane electrode assembly
QA	quaternary ammonium
TFSA	trifluoromethanesulfonic acid
TFA	trifluoroacetic acid
TFAp	2,2,2-trifluoroacetophenone
DPBHF	2,7-diphenyl-9,9-bis(6-bromohexyl)-fluorene
DODPF	9,9-dioctyl-2,7-diphenyl-9H-fluorene
DMDPF	9,9-dimethyl-2,7-diphenyl-9H-fluorene
TMA	trimethylammonium
Qui	quinuclidine
Pip	N-methyl piperidine
bisPip	trimethylenebis(1-methylpiperidine)
DIPEA	N,N-diisopropylethylamine
MeI	methyliodide
DCM	dichloromethane
NMP	N-methyl-2-pyrrolidone
DMSO	dimethylsulfoxide
PAA	poly(arylene alkylene)
aq.	aqueous
SN2	bimolecular nucleophilic substitution
E2	bimolecular elimination
E1	unimolecular elimination
PS	polystyrene

Acknowledgements

This thesis has been performed at the Centre for Analysis and Synthesis (CAS) at Lund University. I have always felt lucky to work in such a wonderful environment and meet amazing, intelligent, and supportive people. I definitely can say that without their help and support, I would not have been able to complete this scientific work. I would like to thank the following people from the bottom of my heart.

My supervisor **Patric**, for giving me the opportunity to complete my Ph.D. research in his group. Your door was always open for me. You have provided me with guidance and support in my research but still given me the freedom to work independently. You taught me a lot about time management, elegant chemistry, prioritizing duties, and communication skills. I learned a lot from your experience and wisdom. I never left your office without motivation.

I would like to thank my co-supervisor Bao, and department representative Ola for their support.

I would like to thank the Polymat group for their help and support as well as for creating a welcoming environment: Anuja, Axel, Carlos, Choi, Christopher, Dang, David, Denis, Dong, Haiyue, Hannes, Huong, Isabell, Joel, Laura, Mikelis, Monica, Narae, Niklas, Nitin, Olivier, Oskar, Pegah, Ping, Rauno, Robin, Sathiyaraj, Si, Smita, Son, Tam, Triet and Xiaoya.

Joel, thank you for your friendly and constructive discussion about research and general topics. I learned a lot from you, but I wish I could also learn to give up on something that is difficult to achieve at the right time. Thank you for the wonderful collaboration.

Huong, thank you for teaching me the methods of polymerization and characterization. You are the person that I have collaborated the most within our group. I have learned a lot from numerous discussions with you; I am now trying not to generalize things.

Hannes, thank you for your attention to details in the labs. I learned a lot from your advice on my research and general topics, as well as during teaching activities.

Dong, thank you for the friendly, constructive discussion about research. I also want to thank you for your attention to details in our lab. We have spent wonderful time not only in Lund but also in Bad Zwischenahn during EMEA 2019. You always got my back.

Pegah, thank you for the friendly, constructive discussion about the research. We have done a lot of work together and you are the second person that I collaborated with the most in the group.

Oskar, thank you for helping with the proofreading of my thesis. I would like to thank you for the constructive discussion we had during lunchtime. I am learning to act Swedish and evaluate situations as a Swede. I wish I could meet you early in my Ph.D. studies so that I would not need to cook at home at all.

Choi, thank you for your friendly, constructive discussion about the SAXS and impedance instrument.

I would like to thank all present and past colleagues at the CAS who have supported me directly or indirectly in completing my Ph.D. studies.

I would like to thank Maria Levin and Sara Röstlund for your helpful administrative affairs, Katarina Frederiksson and KC purchasing office for working tirelessly to supply us with chemicals.

I would like to thank the Swedish Energy Agency, the Swedish Research Council, the Swedish Foundation for Strategic Research, and the Royal Physiographic Society of Lund for their financial support.

I would like to thank my family for their continuous support during my Ph.D. studies. I would like to thank Kujtim Verlaku and his family for theirs. I would like to thank Ada Yakar and her family for their support.

Table of Contents

Introduction

1.1 The fuel cell

Fuel cells have been known as environmentally friendly power sources. The exact date for its discovery is not clear, but it appeared in the beginning of the 18th century[1]. Christian Friedrich Schönbein, a German-Swiss chemist, introduced the fuel cell concept and published the work in Philosophical Magazine in January 1839.[2] In the same year, Sir William Robert Grove, a British physical scientist, published his idea[3], on the Grove cell, in the same journal, but in the February edition[4]. The fuel cell concept is very well-known and in simple terms as converts chemical energy into electrical energy. Since then, fuel cell technology has been studied and developed.[2, 5] Nowadays, the fuel cell consists of two electrodes (anode and cathode) separated by a solid electrolyte which is usually a polymeric membrane.[6] It is essential to mention that this ion exchange membrane is considered to be the heart of fuel cell.[7] The membrane is responsible not only for the transportation of ions from one electrode to another, but also for the separation of the electrodes. [8-10] Depending on the nature of the membrane and the temperature at which they operate, fuel cells can be classified into five categories; proton exchange membrane fuel cells (PEMFCs)[11], alkaline fuel cells (AFCs)[12], anion exchange membrane fuel cells (AEMFCs)[13], phosphoric acid fuel cells (PAFCs)[12, 14], molten carbonate fuel cells (MCFCs)[15], and solid oxide fuel cells (SOFCs).[16] PEMFCs, AFCs, and AEMFCs operate under low temperatures, < 100 °C, and other fuel cells operate under high-temperature conditions, above 150°C.[9] For example, SOFCs' operation temperature is 1000 °C. Importantly, that fuel cells are generally environmentally friendly and highly efficient in energy generation. However, it cannot convert all the chemical energy released from the electrochemical reactions into electricity because of some losses due to ohmic resistance, fuel/current crossover, and activation losses.[17] Another reason for the lower efficiency can be related to the low physical and chemical properties of the conducting ion exchange membrane.[6] The coming section will provide more detailed information on the fuel cells that operate under low-temperature conditions.

1.1.1 Proton exchange membrane fuel cells. (PEMFCs)

PEMFCs are a mature technology and have advanced significantly recently.[6, 9, 18] This technology was applied for the first time in the Gemini space project in the 1960s, and in the last two decades, [19-21] it has been successfully in the

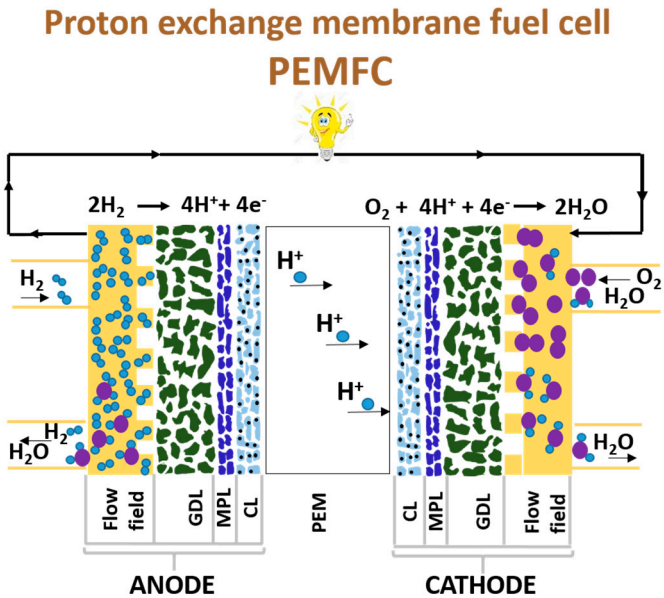

Figure 1. Schematic model of the PEMFC. On the both sides there is a catalyst layer (CL), a microporous layer (MPL), and a gas diffusion layer (GDL).

applied in vehicle. Today, PEMFCs can be seen not only in stationary applications, but also in commercially available cars, such as Toyota Mirai and Hyundai Tucson.[22] Figure 1 presents a model of the PEMFC, which generates electrical power by employing hydrogen and oxygen gases. A fuel cell consists of two electrodes, an anode and a cathode, separated by a solid membrane. The former is responsible for hydrogen reduction reactions and generates protons and electrons.[6] The protons are then transported via the proton exchange membrane (PEM) to the cathode, the electrons generate electric power. The latter is in charge of the oxygen oxidation reactions between oxygen and proton to produce water and complete the total reaction.[6, 23, 24] (Figure 1). The electrochemical reactions are as follows:

Anode (Oxidation) :	$H_2 \rightarrow 2H^+ + 2e^-$	E^0=0 V
Cathode (Reduction):	$\frac{1}{2}O_2 + 2H^+ + 2e^- \rightarrow H_2O$	E^0=1.23V
Total:	$\frac{1}{2}O_2 + H_2 \rightarrow H_2O$	E^0=1.23V

One of the most critical components in this type of fuel cell is the PEM because it separates the two electrodes and is responsible for the transportation of the protons during the fuel cell operation. The most common and well-known PEMs electrolyte employed in the fuel cells of today was invented by DuPont.[25] Nowadays, this membrane is well-developed and known by its trade name Nafion®. Nafion® is a polymer tethered with strong acids, i.e, sulfonic acid groups (-SO_3H) via perfluoroalkyl chains (Figure 2).[25] Distribution of the acids along the polymer backbone and the way they are tethered directly affect the

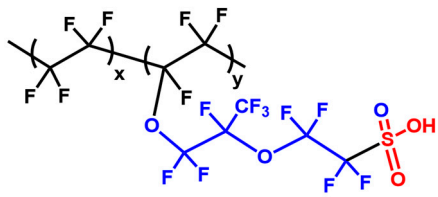

Figure 2. The polymeric structure of Nafion® (adapted from Kusoglu el at.[25])

membrane's morphology and physical and chemical properties. This unique polymeric architecture gives a clear morphology composed of hydrophilic and hydrophobic phase domains, which leads to high proton conductivity.[25] The former promotes the transportation of protons by forming a percolating water-rich phase network. The latter mitigates the excess water in the membrane, which might otherwise impair the mechanical properties of the membrane. However, Nafion® has several drawbacks. First, the solid electrolyte is very expensive to produce ($500 m^2)[22] and is not environmentally friendly. For example, in 2013, the Nafion® membrane was said to be the single most expensive component in a fuel cell stack.[26] Nafion membranes also possess a high fuel permeability, and is challenging to operate at high temperatures ($\geq 90°$) due to poor mechanical properties (low T_g) and high conductivity loss.[26] Lack of fuel flexibility is another drawback; usually, only hydrogen and lower alcohols (methanol or ethanol) can be applied as fuel.[23, 27] Still, the most problematic drawback is the dependence on the precious platinum group metal catalysts necessary for the electrochemical reactions in both anode and cathode.[27, 28] There has been many efforts to replace and decrease the amount of metal catalyst[29] or recycle the platinum for the PEMFCs,[30] but further development

is still required. These stumbling blocks are barriers to commercializing the PEMFC on a large scale.

Alkaline fuel cells (AFC) employing potassium hydroxide as a liquid electrolyte were described for the first time by Reid in 1902, almost 63 years after the concept of acidic fuel cells.[31] AFC was developed a lot since then, and was as part of the NASA Apollo space program in 1950 to generate electricity from hydrogen.[1] Moreover, this technology was applied forklift trucks, and for energy storage.[10] The working mechanism differs from the PEMFC; here, the oxygen reacts with water to produce hydroxide ions in the cathode. The hydroxide ions are then transported to the anode via the liquid KOH solution, where they react with hydrogen to generate water and electrones. The electrons are transported through an external circuit to the cathode, where they are used to generate the hydroxide ions. The reactions taking place in two electrodes are as follows:

Anode (Oxidation) :	$2OH^- + H_2 \rightarrow H_2O + 2e^-$	E^0= -0.83 V
Cathode (Reduction):	$\frac{1}{2}O_2 + H_2O + 2e^- \rightarrow 2OH^-$	E^0= 0.40 V
Total:	$\frac{1}{2}O_2 + H_2 \rightarrow H_2O$	E^0=1.23V.

Operation under an alkaline environment offers AFC significant advantages compared to PEMFC. One of the most important advantages is that AFC possesses a faster oxygen reduction reaction at the anode, resulting in higher electric efficiency.[1, 23] This allows employing a wider choice of non-precious group metal-catalyst such as Ni and Ag for the electrochemical reactions. On the other hand, the use of liquid electrolytes is the main disadvantage of AFC.[32] The KOH solution electrolyte is very difficult to prepare and handle, and it is very corrosive to the catalyst leading to high degradation of these. Lastly, the KOH solution is very sensitive to carbon dioxide (CO_2), decreasing the fuel cell's efficiency. [1, 9, 23] For example, when air is used instead of oxygen, the hydroxyl ions may react with CO_2 and form carbonate ions or potassium carbonate, as it is shown in the following reactions:

$$2OH^- + CO_2 \rightleftharpoons CO_3^{2-} + H_2O \quad (1)$$

$$2KOH + CO_2 \rightleftharpoons K_2CO_3 + H_2O \quad (2)$$

The most compelling cause of the decrease in the performance of AFC is the formation and precipitation of potassium carbonate, K_2CO_3.[23] Firstly, the formation of metal carbonate salt decreases the number of hydroxide ions both in the anode and electrode, thus reducing the efficiency of the hydrogen oxidation reaction.[1]

Moreover, the presence of K_2CO_3 salt in the electrolyte solution changes the composition of the electrolyte by eliminating the OH^- ions in it, leading to a decrease in ionic conductivity.[1, 9] Furthermore, metal carbonate precipitation blocks the pores of the gas diffusion layer and prevents gas diffusion, thus reducing the efficiency of the fuel cell. Another factor affecting fuel cell efficiency is the amount of liquid electrolyte. If the electrolyte amount is in excess, it causes electrode flooding, and if the electrolyte amount is insufficient, it leads to electrode drying.[33, 34] Although CO_2 poisoning of the electrolyte reduces the performance of the fuel cell, the independence from noble metals catalyst (Pt and Pd) is a clear advantage of the hydroxide ion-based fuel cell. [35]Changing the electrolyte from liquid to solid form generates a new type of fuel cell named anion exchange membrane fuel cell (AEMFC), which will be discussed in the next section.

1.1.3 Anion exchange membrane fuel cells (AEMFCs)

AEMFCs have the same working principle as AFC with only one difference. Here, a solid electrolyte is employed for the electrode separation and OH^- ion transportation (Figure 3) instead of a liquid electrolyte. The solid electrolyte is considered the heart of the fuel cell and is named the anion exchange membrane (AEM).[36] The AEM consists of a polymer backbone and a cationic groups tethered covalently to it serving as counter ions for the hydroxide ions.[37]

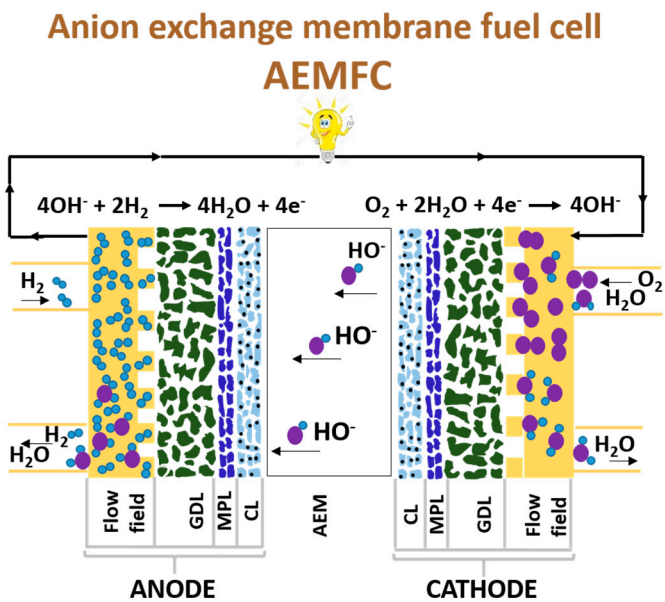

Figure 3. Schematic model of the AEMFC. On both sides there is a of catalyst layer (CL), a microporous layer (MPL), and a gas diffusion layer (GDL).

The cationic group attached to the polymer backbone eliminates the formation and precipitation of metal carbonate salt, which tends to block pores in the gas diffusion layer.[23] In addition, the AEMFC technology allow usage of a wider range of fuels, such as ethanol, propanol, and pure hydrogen, to generate electric power.[23] Notably, hydroxide ions in the solid polymer electrolyte react completely with CO_2 within 10 minutes after exposure to air,[27] generating bicarbonate and carbonate ions according to:

$$OH^- + CO_2 \rightleftharpoons HCO_3^- \quad (3)$$

$$OH^- + HCO_3^- \rightleftharpoons H_2O + CO_3^{2-} \quad (4)$$

Of course the formation of these ions negatively influences the performance of the cell. Research on AEMs started in 2006 when Varcoe and coworkers published the pioneering work on the solid electrolyte fuel cell.[38]

There are other properties of the membrane, such as mechanical, thermal, and chemical stability, which directly affect the performance, durability, and cost of the fuel cell. [21, 37, 39-44] Therefore, it is important to know which properties that affect fuel cell operation and how. For example, the AEM has two essential functions: to allow the transportation of the ions and prevent fuel and electrons to pass. [45] Hence, one of the important properties of a membrane is the have high ionic conductivity and low, or almost no, fuel and electron transport.[23, 46-48] Additionally, the fuel cell generates electricity under very harsh conditions: high pH medium at elevated temperature (90 °C). Therefore another crucial characteristic of the membrane is a sufficiently high and long–term chemical and physical stability.[49-52] Moreover, the membrane should be thin to reduce the ohmic loss and facilitate efficient water management. [1, 23] Finally, the AEM should be environmentally friendly, in expensive, and easy to recycle or reuse. It is essential to mention that all desired (challenging) properties of AEMs have a close relationship with the polymer backbone architecture and its composition, the cationic group and its structure, and how the cationic group is tethered to the polymer backbone.[36, 37, 40-45, 53-55] The coming section will be focused on the challenges of anion exchange membrane desins.

1.2. Challenges for anion exchange membranes

As mentioned above, high ion conductivity and long-term chemical stability are essential properties of anion exchange membranes for application in fuel cells and water electrolysers. However, until now, the commercially available membranes possess a lower ion conductivity and low thermochemical stability compared to the proton exchange membranes with the same ion exchange capacity. These two essential features of the membrane strongly depend on the polymer backbone architecture and the nature of the cationic group.

1.2.1 Hydroxide conductivity

Ion exchange capacity

Ion exchange capacity (IEC) is determined as the number of cationic groups (molar equivalence) per unit mass of the dried polymer.[53] Increasing the value of IEC is a simple strategy to improve the hydroxide conductivity. Moreover, membranes with high IEC take up a lot of water, which is essential for forming percolating channels to facilitate the transport of hydroxide ions toward the anode.[56] However, an excess water uptake and dimensional swelling are usually accompanied not only by a dilution of the cations, which decreases the ionic conductivity drastically, but also by the deterioration of the mechanical properties of the membrane.[57, 58] Another strategy to enhance the ionic conductivity of the membrane without sacrificing the mechanical properties is to synthesize a polymer architecture with a well-developed morphology, which promotes the phase separation and formation of ionic clustering.[56, 59-61] Both are very important for creating interconnected ionic channels, which facilitates the movement of hydroxide ions.

The mobility of hydroxide ions

The low ionic conductivity of AEMs is associated with the comparatively lower mobility of hydroxide ions due to size and solvation differences compared to proton. For example, OH^- ion is hyper-coordinated by ~4.5 water molecules, while the proton is hypo-coordinated by 3 water molecules.[62] The hydroxide ions tend to possess durable solvation shells by reorganizing the water molecule and breaking the hydrogen bond network, while the hydronium ions are easily integrated into the hydrogen bonding network.[63] Therefore, the mobility of hydroxide ions is 1.75 times lower than proton cations in liquid water at room temperature.[62] In addition, the water self-diffusion is very important to generate the hydrated phase domain and promote anion transportation.[64] The water self-diffusion coefficient in anion exchange membranes is higher than the bulk water self-diffusion, indicating that the water is less bound to the polymer and diffuses faster in the membrane, leading to reduce hydroxide transportation.[65] On the contrary, the water self-diffusion is lower than bulk water diffusion in proton exchange membranes, implying that water is stronger bounded with the polymer and diffuses slower in the membrane.[65] This leads to the generation of the hydrated phase domain, which facilitates proton transportation. [66]

Transport mechanism

It is considered that the Grotthuss mechanism, diffusion, migration, and convection is the most dominant transport mechanism of hydroxide ions.[1] Grotthuss's mechanism explains the diffusion of OH^- ions through water molecules, which is occurs via the formation/cleavage of hydrogen bonds. It is suggested that the transportation of hydrated hydroxyl ions is guided by hyper-coordinated four-water

molecules ($H_9O_5^-$).[67] The water molecules are necessary for the formation/cleavage of covalent bonds between the hydroxyl ions and water during the hydroxide transportation. [64, 66]

Morphology

As was mentioned above, the weaker interaction between the quaternary ammonium and water molecules increase the diffusion of water in the membrane preventing the efficient formation of ionic clusters. An alternative approach to generate ionic clustering and improve the phase separation (hydrophobic/hydrophilic phase) is to change the architecture of the polymer molecule.[37, 43, 44, 53, 68] Common strategies to improve the phase separation and enhance the ionic clustering of the polymer include employing an alkyl chain,[69] grafted side chain,[70, 71] block copolymer,[72] and charge localization. [73]

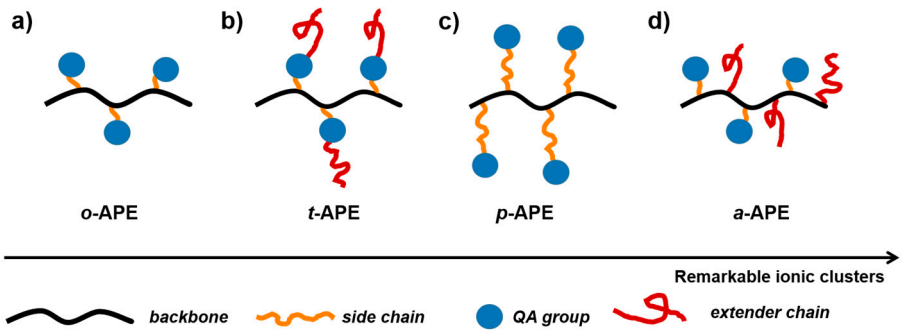

Figure 4. Schematic illustration demonstrating different strategies used to enhance the formation of ionic clusters in alkaline polymer electrolyte (APE), a) original structure of tethering cationic group to the polymer backbone (*o*-APE), b) Tadpole type where the extender chain is attached to the cationic group (*t*-APE), c) pendant-type, the cationic group is attached to the polymer backbone via hydrophobic alkyl side chain, and d) new-style, the extender chain and cationic group are attached separately on the polymer backbone (a-APE) (adapted from Pan and Zhuang et al.)[73].

Pan and Zhuang et al. have investigated the formation of ionic clustering in different polymer architectures where the cationic group and alkyl chain are tethered separately on the polymer backbone, as shown in Figure 4.[73] Next, a computational screening was carried out using coarse-grained molecular dynamics (CGMD) simulations to determine which of the polymer architectures above was the most efficient ion-aggregating structure. The backbone segment, quaternary ammonium hydrated hydroxide ions, alkyl chains, and water clusters were used to build APE systems at a dry level (λ=4) and a fully hydrated level (λ=20). The CGMD results showed that in both dry and fully hydrated conditions, all of the simulated structure factors in all the APE series showed a peak in their curves. In both hydration levels, the *a*-APE showed the sharpest and strongest peaks, indicating a clear pattern for remarkable ionic clustering. However, the *a*-APE polymer architecture is not very

stable in the alkaline environment because the cationic groups (QA) are attached in the benzylic position.[13]

In the Pan and Zhung investigation, the *p*-APE polymer structure also exhibited a clear and sharp peak, implying another approach to facilitate ionic-cluster formation. Moreover, introducing the cationic group via the alkyl chain enhances the alkaline stability of the cation because of the absence of benzylic protons. Introducing cationic groups via alkyl chains in the polymer backbone is synthetically challenging.[23]

Another strategy to facilitate phase separation and enhance the ionic conductivity of the membrane is to increase the local cationic concentration, i.e., by using multicationic repeating units.[74, 75] However, placing cationic groups too close, i.e., with less than 4 methylene groups between two cation groups, showed a decrease in the ionic conductivity.[75] This can be attributed to incomplete ionic dissociation.

1.2.2 Alkaline stability

Poor chemical stability under high pH conditions at elevated temperature is a serious obstacle to the development of AEM. It limits the application of the membrane as an electrolyte in fuel cells. The degradation of the membrane is directly connected to the structure of the polymer backbone,[76, 77] the linkage used to tether the cationic group to the polymer backbone,[78, 79] and the cationic structure.[80] Among them, the design of the cationic group is considered the most significant factor because its degradation reduces the IEC and drastically decreases the ion conductivity and the performance of the fuel cell. Quaternary ammonium (QA) groups are the most investigated functional group due to several reasons.[42, 53, 81] QA groups are economically affordable, commercially available, and are relatively easy to be prepare. Moreover, QA groups have high ionic conductivity and good alkaline stability. Figure 5 shows possible degradation mechanism routes of the QA in an alkaline environment. Under the alkaline media at elevated temperature conditions, QA cationic groups are prone to OH^- attack leading to degradation by nucleophilic substitution (S_N2), Hofmann elimination (E2), E1 elimination, ylide formation, and chemical rearrangement (Figure 5).[1, 56]

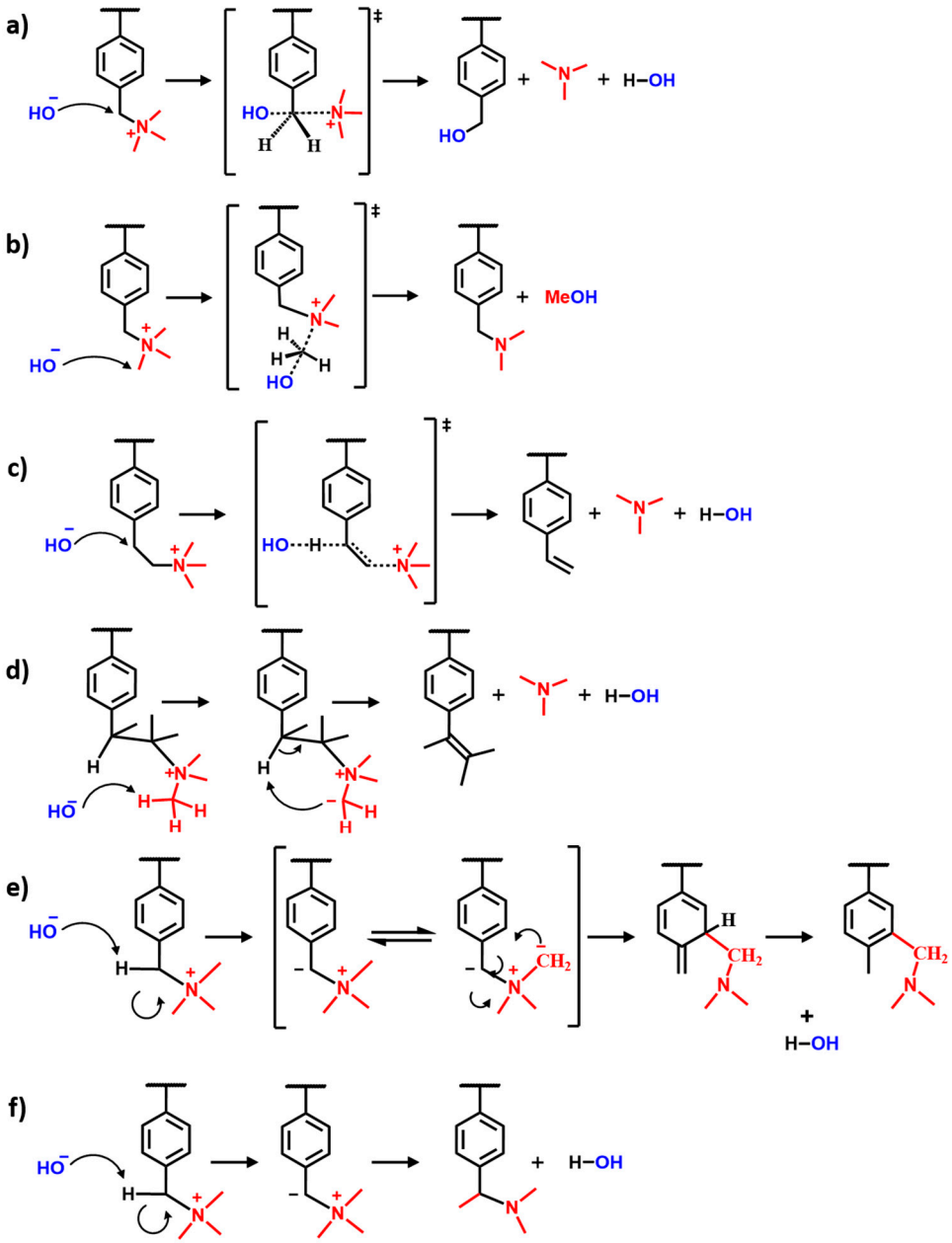

Figure 5. Chemical degradation pathways of QA cations a) nucleophilic substitution at benzyl position, b) nucleophilic substitution at methyl position, c) Hofmann elimination (E_2), d) E_1 elimination, e) Sommlet-Hauser rearrangement, and f) Stevens rearrangement.

The most common degradation pathway is nucleophilic substitution in benzylic positions (Figure 5a) and methyl group (Figure 5b), followed by Hofmann elimination via β-hydrogens (Figure 5c). During nucleophilic substitution reactions, the hydroxide ion, a strong base and a nucleophile, attacks at the α-carbon, which is an electron-poor carbon, leading to the formation of an alcohol and a tertiary amine group. Moreover, the rate of nucleophilic substitution reaction depends on the type of the carbon, the order as primary carbon (1° C) > secondary carbon (2° C) > tertiary carbon (3° C) > quaternary carbon (4° C).[55] Another critical factor that significantly influences the nucleophilic substitution rate is the concentration of the nucleophile (OH^- ions); the higher the concentration of OH^- ions, the higher the reaction rate (Figure 5a and b).[55]

The Hofmann elimination reaction requires a β-hydrogen in anti-coplanar conformation. As clearly seen in Figure 5c, the hydroxide attacks the β-protons to produce an alkene, tertiary amine, and water. Moreover, the rate of reaction in Hofmann elimination is 4° C > 3° C > 2° C > 1° C.[55] E1 elimination reaction can also occur when there is a steric hindrance at α- and β-positions of the ammonium group (Figure 5d). Introduction of steric hinderance group by e.g, methyl groups results in the formation of stable intermediates, which favors E1 elimination reactions.

Finally, in some instances, the QA group can degrade via ylide formation: Sommelet-Hauser rearrangement and Stevens rearrangement (Figure 5e-f).[23]

In addition, in parallel with the investigation of the cations, researchers have also focused on the polymer backbone structure employed in AEMs. The polymer backbone plays an essential role in the design of AEM because it directly affects the physical and mechanical properties of the AEM and also influences the alkaline stability of the cationic group.[54, 57, 82, 83] At the beginning of, common polymers such as polysulfones and poly(ether ketone)s were applied as the backbone due to the easy access, low cost, and straightforward synthesis.[42] Moreover, these polymer architectures possess good mechanical and thermal stability, good film-forming properties, and straightforward modification chemistries, e.g., the introduction of cations in the benzylic positions. [41, 43, 84] However, these traditional polymer backbones are generally not chemically stable under alkaline conditions and exhibited signs of degradation in the polymer backbone. Cationic moieties located in the ortho position on aromatic ring delocalize the vicinal electronic structure by pulling the electron from the rings.[53] This drastically accelerates the hydroxide attack and triggers backbone degradation (Figure 6).

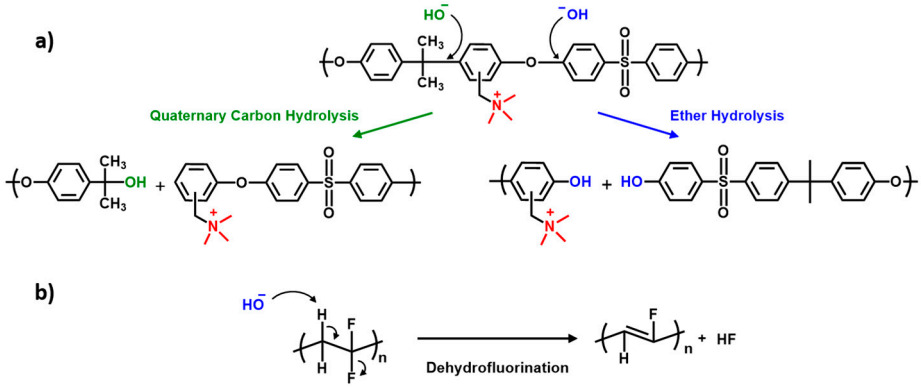

Figure 6. Degradation pathways of polysulfone (a) and polyvinylfluoride (b)(modified from Ladewig et al[53]).

The prodcuts are quaternary carbon hydrolysis and ether hydrolysis (Figure 6a). Moreover, sulfone linkage has an electron-withdrawing effect on the para position which activates and supports the degradation of the polysulfone backbone.[42, 44]

Additionally, fluorinated polymers such as poly(vinylidene fluoride) have been suggested. However, they were vulnerable to hydroxide attack in an alkaline environment leading to dehydrofluorination and the formation of double bonds (Figure 6b).[53]

1.3 Strategies to improve AEM properties

As pointed out in the previous section, poor alkaline stability trigger the degradation of the polymer backbone and the cationic functional group. Moreover, insufficient ionic conductivity due to the effect of IEC and the transporting mechanisms is a further challenge in the AEM research. Both issues are influenced by related to the cationic group, polymer backbone, and how the cationic component is tethered to the polymer backbone, as well as the morphology of the polymer. This is discussed in detail in this section.

1.3.1 Cationic group

The organic cationic groups, covalently bonded to the polymer backbone, are essential in the AEM because they serve as counter ions for the hydroxide ions. However, these head groups are susceptible to hydroxide attack and degrade in different ways (see Figure 5). Hence, many research groups have focused on investigating different cationic groups for AEM, and improving and enhancing their alkaline stability in alkaline environment. The cationic groups investigated to date

can be classified as nitrogen-containing, nitrogen-free, and organic metal cationic groups (Figure 7).[44] Nitrogen-containing groups can be divided into sub-groups, such as ammonium cations and N-conjugated cations.

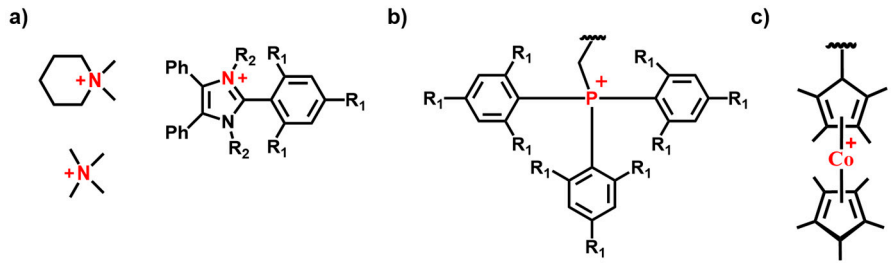

Figure 7. Chemical structures of nitrogen containing cationic groups (a), a nitrogen-free cationic group (b), and an organo metalic cationic group (c).

Marino and Kreuer investigated the half-life times of 26 different low molecular weight quaternary ammoniums cations under very harsh alkaline conditions, 6 M aq. NaOH at 160 °C [85]

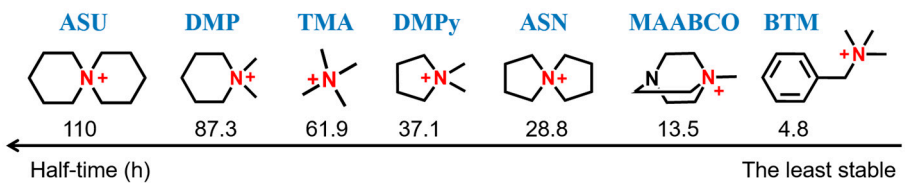

Figure 8. Half-life time of low molecular weight QA after storage in 6 M aq. NaOH at 160°C. [85]

They reported that aliphatic heterocyclic QA groups such as azonia-spiro[5,5] undecane (ASU) and monocyclic N,N-dimethylpiperidinium (DMP) showed the longest times half-life of 110 and 87.3 h, respectively (Figure 8).[85] Benzyl trimethylammonium (BTM) is considered a benchmark in the field and it showed the shortest half-life time , 4.8 h, in this investigation.[85] The authors declared that the outstanding alkaline stability of ASU and DMP was due to the geometrical constraint of the ring, which does not support an anti-periplanar position with favorable bond angles and bond lengths during the elimination transition state.[85] The degradation mechanism for DMP can be nucleophilic substitution on methyl group, on α-carbon in the ring, and Hofmann elimination in the ring (Figure 9).

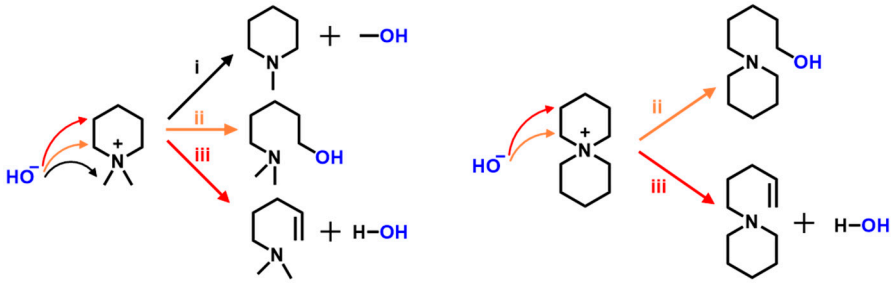

Figure 9. Degradation pathways after storage in 6 M aq. NaOH solution at 160°C of DMP (left) and ASU (right) cations: nucleophilic substitution at methyl group (1), ring-opening substitution (ii) and ring-opening β-elimination (iii).[85]

In order to reduce the activity of the β-hydrogen, the author suggested using a cage-like structure of quaternary ammonium groups such as 1-methyl-4-aza-1-azonia-bicyclo[2.2.2]octane, MAABCO, where the β-hydrogens are locked into non-anti-planar position. However, as can be seen from Figure 8, it is less alkaline stable than TMA, with a half-life time of 13.5 h. The reason can be related not only to the second nitrogen, which has electron-withdrawing properties and is closer to the positive charge, but also to the ring strain. If the additional nitrogen is replaced with carbon atom to obtain quinuclidine, it possesses the same cage-like structure and may increase the alkaline stability due to maintaining the rotational inhibition.[85] Furthermore, Lee and coworkers investigated the electronic effect of substituents on N-heteroatoms (NHA) groups under different λ, i.e., the number of water molecules per cationic group, at λ = 4.8, 7, and 10 at 80 °C.[55] They applied ^{1}H-NMR spectroscopy to analyze the degradation mechanism. In all λ conditions, ASU and DMP cations showed outstanding alkaline stability due to a constrained configuration and highly symmetric structure. At λ = 4.8 conditions, NHA with electron-withdrawing substituents (heteroatom or phenyl) at a α- and β-position (DM-IQ, IS-ASU, O-DMP, O-ASU) increased the rate of nucleophilic and Hofmann elimination reaction drastically compared to non-substituted ASU and DMP (Figure 10). However, when electron-withdrawing substituents were tethered at the γ-position (Bis-TA-DMP and Bis-TA-ASU), the alkaline stability of the cation improved significantly compared to the compounds with electron-withdrawing substituents tethered at α and β-position due to the decreased electron-withdrawing effect (Figure 10).[55]

NHA groups tethered with electron-donating substituents (CH_3, CH_2, and benzyl) in α, β, and γ-positions, increased the steric hindrance and electron density of the N-heterocyclic rings, mitigating the reactivity of S_N2 and E2 reactions.[55] Additionally, the electron-donating substituents attached in the γ-position of the NHA group showed higher alkaline stability than electron-donating substituted in α- and β-positions. Moreover, ASU and DMP showed the highest alkaline stability due to their symmetrical structure and geometric conformations.[55]

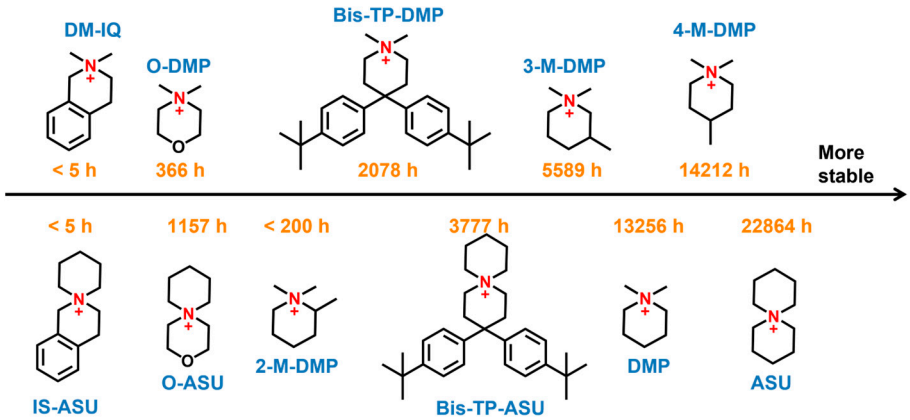

Figure 10. Stability of different QA under λ = 4.8 conditions at 80 °C analyzed by ^{1}H NMR spectroscopy.Modofief from Lee el at.[55]

Several N-conjugated ammonium cations have been investigated for use in AEMs.[86] Among them, imidazolium and benzimidazolium-based cations are considered the most promising candidates due to their excellent alkaline stability.[87] The positive cation is delocalized between C2 and nitrogen atoms (N1 and N3) in an aromatic heterocyclic ring.[88-90] Imidazolium mainly degrades via a ring-opening mechanism. Therefore, introducing electron-donating substituents at the C2 positions is considered the most effective way to enhance the alkaline stability of imidazolium.[91, 92] The electron-donating group increases the electron density and generates a steric hindrance at C2, which mitigates the reactivity of the nucleophilic substitution, and prevents the ring-opening of imidazole.[90] In 2019, Fan et al. investigated the N-conjugated imidazolium cationic groups and reported that the bis-arylimidazolium[93] (Figure 11b) and arylimidazolium[93] (Figure 11c) possess the highest alkaline stability with a half-life of more than 10000 h under very harsh alkaline treatment, λ = 4.8 at 80 °C.[82, 93] The author reported that the outstanding alkaline stability is related to the bulky structure and steric hindrance of the arylimidazolium. However, the bulky design of the N-conjugated cationic group has many limitations. Many steps are involved during the synthesis process, leading to an increase in the cost.[45, 55]The bulky heavy structures decrease the IEC value, resulting in low ionic conductivity. Lastly, it is challenging to integrate this structure into a polymer backbone.

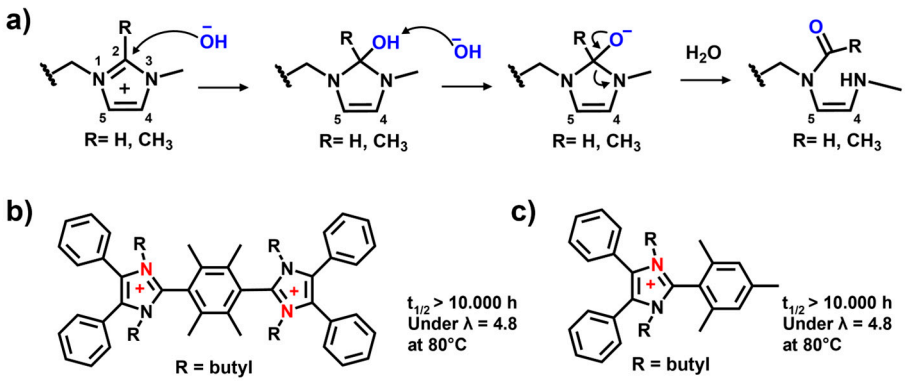

Figure 11. Degradation pathway of imidazolium (a), the chemical structure of bulky bisarylimidazolium[93] (b), and arylimidazolium[93] (c).

Nitrogen-free cations such as phosphonium have been the subject of several investigations.[23, 43] Phosphonium cations degrade via a nucleophilic attack on the phosphorous center, generating phosphine oxidation.[42] To enhance the alkaline stability of the phosphonium cation, bulky and electron-rich structures, such as methoxy-substituted aromatic compounds are introduced on the phosphorous atom.[94-96] However, as mentioned before, bulky structures decrease the IEC resulting in low ionic conductivity.

The organometallic centers have been investigated as cationc groups by several researchers. Cobaltcenium has shown an attractive alkaline stability. However, most of the organometallic groups lost ligands in alkaline solution and exhibited poor AEMFC performance.[43]

How the cationic group is attached to the polymer significantly influences the degradation of the cationic moieties. Tethering the cationic groups to the polymer backbone via an alkyl chain (>4 carbon) has been reported as an excellent strategy to improve the alkaline stability.[69, 81, 97, 98] Furthermore, introducing cationic groups via alkyl chains onto the polymer backbones avoids the benzylic position, which is considered an unstable position, and increases electron density at the β-hydrogen.[81, 99, 100] This generates steric hindrance and reduces the possibility of the Hofmann elimination reaction. Marino and coworkers have investigated the effect of alkyl chains on the half-life times of different low molecular weight QA salts. [85] They reported that the half-life time of an ethyl group was very short and significantly increased when an alkyl spacer was between 3-6 carbon atoms long. A rapid degradation was observed when QA was attached to the benzylic position in the backbone. [81, 85] The authors suggested that the quick degradation of the ethyl group is related to many factors, for example, lack of steric hindrance at the β-protons,

availability of freely rotating β-protons, and that the cationic group increased the acidity of the β-protons.

1.3.2 Polymer backbones

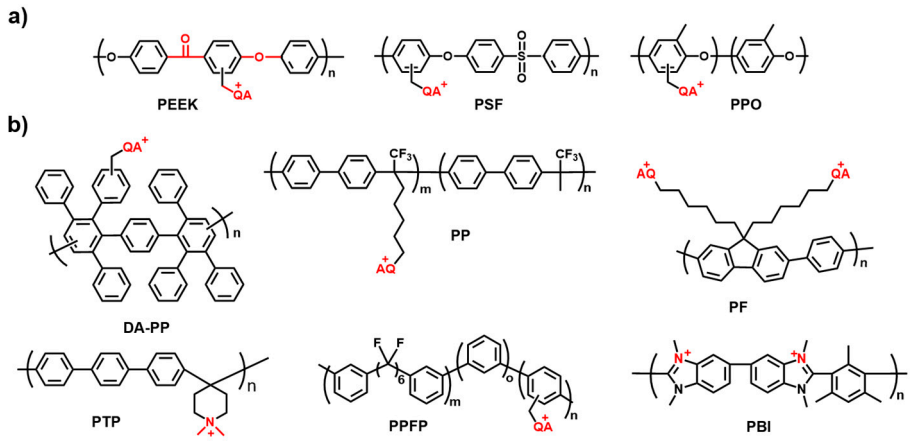

Figure 12. Molecular structure of different functionalized polymers a) arylether-containg polymers and b) aryl ether-free polymer.[54]

The polymer backbone is responsible for the mechanical robustness and toughness of the membrane during cell operation. It also significantly affects the water uptake and ion conductivity of the membrane. Operating in alkaline media, the polymer backbone is prone to hydroxide attack and degrade.Initially, well-known polymer architectures with good mechanical and thermal stability properties, such as poly(ether ketone) (PEEK),[101] polysulfones (PSF),[102] and poly(phenyl oxide) (PPO)[103, 104], were used as a backbone to covalently tether cationic groups to (Figure 12a). Although the ether bridge enhances the solubility due to low rotational barrier, are very sensitive to OH^- attack and lead to backbone cleavage in alkaline media at elevated temperatures (Figure 6a).[105]

One of the most efficient approaches to enhance the alkaline stability of polymer backbone is to synthesize ether-free aromatic polymer architectures. [43, 45, 54] It is important to mention that aromatic polymer backbones generally have a high glass transition temperature, good thermal and alkaline stability, high impact strength and toughness, and low water uptake compared with polymers without an aromatic structure.[54] There are not many commercially available ether-free polymer backbones available. Therefore, many synthesis procedures have been developed to generate a variety of polyaromatic backbone architectures, (Figure 12b). The Diels-Alder reaction was employed to synthesize a polymer with six pendant phenyl groups per repeat unit attached randomly in *para* and *meta* positions (Figure 12b, DA-PP).[13, 98] The random configuration enhances the solubility of the polymer in

organic solvents, facilitating the functionalization and characterization process. Diels-Adler polymerizations have several advantages. The reaction is run under metal-free conditions, avoiding the contamination of the final product. The final product possesses good solubility leading to easy processability. On the other hand, the required of a multi-step process for post-functionalization and the need for high molecular weight to reach good mechanical properties can be considered drawbacks of this technique.[54] Transition-metal-catalyzed cross-coupling reaction, i.e., the Suzuki coupling reaction, is another method used to produce ether-free polyaromatic polymer backbones. Lee *et al*. synthesized ether-free fluorene-based copolymers (PF) via a Suzuki coupling, where the functional group was introduced via an alkyl chain.[52] Later, Miyatake *et al.* synthesized a polymer structure consisting of perfluoroalkylenes and quaternary oligophenyl groups via nickel-catalyzed coupling reactions (PPFP).[106, 107] The perfluoroalkylene copolymer exhibited a high polydispersity (PDI) indicating the difference in the reactivity between aryl halides.[107] Suzuki-coupling reactions have been considered an excellent alternative to generate different and ether-free polymer architectures with good mechanical, thermal, and alkaline stabilities. However, the requirement of palladium metal catalyst and boron-containing monomers are downsides of this technique.[54] Holdcroft *et al.* produced highly alkaline-stable polymer backbones based on the steric hindrance of benzimidazolium units (PBI, Figure 12b)[108]. The polymer provides a high IEC value due to the small molecular weight of the repeating units, making the polymer soluble in water and limiting the usage as AEMs.[108] Super acid-catalyzed polycondensation reaction between a ketone and arenes to generate a C-C bond is another method to synthesize linear and high molecular weight polymers.[109] Lee *et al.* synthesized poly(phenyl alkene) polymers with a cationic group tethered via an alkyl chain (PP, Figure 12b).[51, 110] Jannasch *et al.* produced poly(arylene piperidinium) polymers employing *N*-methyl-4-piperidone and *p*-terphenyl as ketone and nucleophile respectively, via superacid-catalyzed polyhydroxyakylation reactions (PTP).[111] The authors emphasized that the PTP polymer possesses poor solubility due to the p-terphenyl, which stiffers molecular structure in the polymer backbone.[111] This method offers several advantages; (i) metal-free conditions, (ii) simple one-pot synthesis, (iii) generating a flexible polymer backbone due to sp3 hybridization.[54] By introducing the ether-free polymer backbone architecture, the alkaline stability of the membrane has been significantly improved.

The mechanical robustness and flexibility of the membrane are directly related to the molecular weight of the polymers. The higher the molecular weight, the better the intermolecular chain entanglement, which directly enhances the polymer membrane viscoelastic property. However, high molecular polymers lower the processability.[54] The polymer (in a quaternized form) should be able to form a thin film (≤ 30 μm).[54] For example, a number-average molecular weight of $M_n > 50$ kg mol^{-1} is needed for a

linear aromatic polymer backbone to form a flexible membrane. The more bulky structure appeared in the repeating unit of the polymer (DA-PP), the higher the molecular weight should be for casting flexible membranes.[54]

1.3.3 Architecture of the polymer backbone

The architecture of the polymer backbone is of fundamental significance because it influences mechanical properties, thermal and chemical stabilities, water uptake, and ionic conductivities.[46] Ether-free polymer backbones generally improve thermal and alkaline stability and mechanical property.[53, 112-116] It is widely accepted that the formation of ionic clusters and water channels facilitate hydroxide transportation through the membrane.[22, 45-47, 73] Moreover, phase separation decreases the water uptake, resulting in more mechanically robust membranes.[117] Introducing the cationic group via an alkyl spacer to the polymer backbone is considered a very efficient strategy to promote nanophase separation between the hydrophobic backbone and the hydrophilic ionic groups. [69, 76] Another strategy is to increase the local ionic concentration on the polymer backbone.[43, 74, 75] Although synthetically challenging, block copolymers and grafted side chains have been applied to generate phase separation and increase the ionic conductivity. [72, 118] Another approach strategy can be to use crosslinkers chains.[74, 82] Crosslinkers support the mechanical properties of the membrane as well as decrease the water uptake.

1.4 Approach and aim of the present study

This study aims to design and synthesize anion exchange membranes that are suitable for application in fuel cells and water electrolyzers. Based on the knowledge obtained from literature, different methods have been applied to synthesize novel and robust polymer architectures with QA cationic groups as anion exchange membranes. Later, membranes were characterized with respect to water uptake, OH^- conductivity, morphology, and thermal and alkaline stability. The results helped us to understand the relationship between the polymer architecture and polymer properties. Different important factors have been taken into consideration before designing the polymer backbone structure. Ether-free fluorene-based polymer backbone structures were synthesized via an acid-promoted polycondensation reaction. The introduction of different N-heterocyclic ammonium cations via alkyl chains was investigated. Moreover, increasing the local ionic concentration by introducing dual piperidinium groups was successfully carried out. Another important factor that significantly influence the alkaline stability of the cationic group is how it is attached to the polymer backbone. Piperidinium-based cationic groups were tethered in the 4- position to the polymer backbone via an alkyl chain.

Experimental methods

2.1 Monomer synthesis

2.1.1 Alkylation reaction

Alkylation reactions are usually used to transfer one or more alkyl groups to a molecule by replacing hydrogens with the help of a base. In this work, alkyl chains were introduced to fluorene molecules employing a strong nucleophile. The fluorene is commercially available and inexpensive. Fluorene consists of two phenyl rings attached with a methyl bridge.[119] Fluorene possesses a rigid planar structure and outstanding thermal properties. The two acidic protons (C-H) in the methylene bridge allow to introduce different functional groups via alkylation reactions[120]. The reactivity of the C-H bond at the 9-position is essential for the alkylation reaction. It depends strongly on the substituent group attached to position 2 and 7.[119] For instance, the reactivity of these protons for unsubstituted fluorene molecules is extremely weak compared to fluorene.

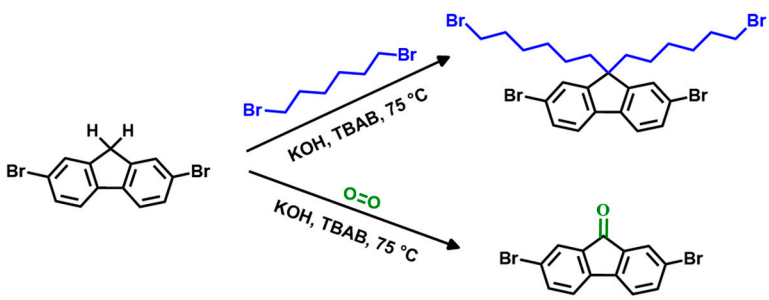

Figure 13. Alkylation reactionof dibromo fluorene with 1.6 dibromohexane[113] (top) and fluorene formation (bottom) [119].

substituted with electron-withdrawing groups such halogen. An alkylation reaction was performed using an excess of 1,6-dibromohexane. A 45 wt% aq. KOH solution and tetrabutylammonium bromide (TBAB) was employed as nucleophile and phase transfer catalyst, respectively. The amount of the phase transfer catalyst has an essential role in facilitating the alkylation reaction; the amount should not be less than 10 mol %.[119] The reaction should be run under nitrogen to prevent the formation of the fluorenone (Figure 13).[119]

2.1.2 Suzuki coupling reactions

A cross-coupling reaction is an organic reaction between organometallic reagents and organohalides to form a C-C bond in the presence of a base and metal complexes such as palladium (0) complexes.[121] These coupling reactions are also known as Suzuki-coupling and Suzuki reactions. The first scientific

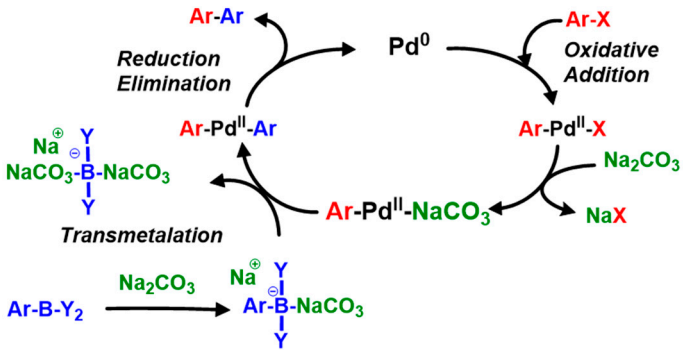

Figure 14. General mechanism for Suzuki coupling reaction between organometallic compounds and organohalides.

publication related to the cross-coupling reactions in the presence of palladium was written in 1979 by Noble laureate Akira Suzuki (2010).[122] Since then, Suzuki-coupling reactions have been developed and are considered not only a powerful technique to produce C-C bonds, but also play an important role in developing synthetic transformations in organic chemistry.[123] Suzuki coupling reactions proceed with a catalytic cycle of three important steps, oxidative addition, transmetalation, and reductive elimination (Figure 14).[124] The oxidation addition step is connected with the oxidation of the Pd(0) to Pd(II), which in many cases is considered the rate-determining step. Pd(0) catalyst is coupled with alkenyl, alkyl, or aryl halide to produce a stable trans-palladium(II) complex. It is important to emphasize that alkyl halides with a β-hydrogen possess a slow oxidation addition to Pd(0) and facilitates the β-elimination reaction rather than Pd(II) complex reaction. However, if a bulky, electron-rich phosphine ligand such as PCy_3 is used, it facilitates the formation of the palladium complexes reaction and makes the coupling of alkyl halides possible. Additionally, alkyl halides relative reactivity decreases in this order I > OTf > Br >> Cl. Many palladium complexes have been used, $PdCl_2(PPh_3)_2$ and $Pd(OAc)_2$, but the $Pd(PPh_3)_4$ is the most useful. Phosphine ligands are widely used because they are stable in air and facilitate the oxidation step by increasing the electron density of the palladium center.[125] Moreover, in Suzuki coupling reactions, the base plays a vital role; in the absence of it, there is no reaction. The base acts as a nucleophile, displacing the halogen from the metal center, and forms the *trans*-Ar-Pd-$NaCO_3$, complex (Figure 14). The base reacts with organoboronic acids and generates borate anions which are important

complexes for the transmetalation step. Moreover, the base is responsible for the promotion of the reduction elimination step, which produces the desired component (Ar-Ar) and a Pd(0) species from the trans- ArPd(II)Ar complex, probably via the addition of a base as the fifth ligand. The final step is the reduction elimination step, in which a Pd(0) complex is generated, and the catalytic cycle is completed. Suzuki coupling reactions can also be applied for sp3-hydridized organometallic reactions with alkyl halides by employing an electron-rich phosphine ligand. [126] Sp3-hybridized organometallic compounds are synthesized via hydroboration of alkenes in the presence of the 9-borabicyclo[3,3,1]nonane (9-BBN) and base.[126] The hydroboration of alkene reaction tolerates different functional groups and proceeds through cis anti-Markonikov addition. Sp3-hybridized organometallic compounds allows for synthesis of monomers where the piperidinium is attached on the 4-position (Figure 15). Suzuki coupling reactions possess many advantages. These cross-coupling reactions proceed under mild reaction conditions, are facile to perform, and maintain a good regioselectivity.[127] Reactants such as organometallic components are very attractive because they are inexpensive, commercially available, and thermally stable chemicals. Moreover, these reactants are inert in the presence of water, tolerate a broad range of functional groups, and give a high yield.[113]

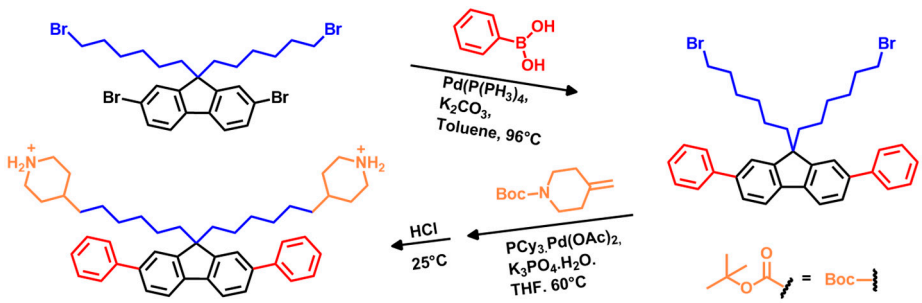

Figure 15. Aryl-aryl Suzuki coupling of aryl-aryl component[113,] (top) and alkyl alkyl Suzuki coupling (bottom). [116]

Additionally, environmentally friendly solvents like water can be employed. After the reaction, the inorganic by-products are not toxic and can be easily removed from the reaction mixture. All these advantages make the Suzuki coupling reaction very useful for forming C-C bonds in the laboratory.

2.2 Polymer synthesis

2.2.1 Acid-mediated polyhydroxyalkylation

The incorporation of fluorine atoms in the polymer structure leads to a macromolecular structure with high-temperature performance and unique chemical properties.[128] There are many methods to incorporate the fluorine group in a polymeric structure. Monomers containing the fluorine, can easily be polymerized via a polyhydroxyalkylation reactions, which are condensations of a ketones or aldehydes with aromatic components in acidic media.[129] The theory of electrophilic activation was first suggested by Nobel laureate G.A. Olah et al. They reported that the reactivity of electrophilic species could be drastically increased in superacidic media.[130] The polyhydroxyalkylation reaction is simple, highly efficient, and can be employed to successfully synthesize linear polymers with high molecular weight.[131-133] Moreover, metal-free conditions and one-pot preparation generate wide possibilities to product a range of ether-free polymer structures by utilizing inexpensive and commercially available monomers.[134] In this thesis, various ether-free polymer backbones were successfully synthesized using the superacid-mediated polyhydroxyalkylation reactions. The reaction was run in one pot using 2,2,2-trifluroacetophenone (TFAp) as a carbonyl reactant, and fluorene-based monomer as an electron-rich nucleophile. A mixture of a strong acid, trifluoromethanesulfonic acid (TFSA), and dichloromethane (DCM) was used as a solvent.

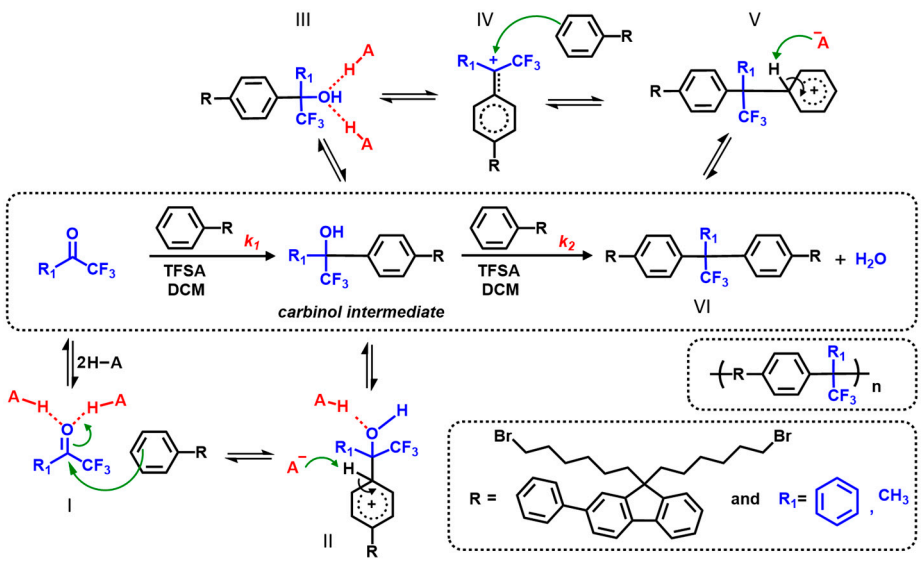

Figure 16. Mechanism of hydroxyalkylation reactions between an aromatic component and a carbonyl component.

The mechanism of an acid-catalysed hydroxyalkylation reaction is shown in Figure 16.[128] The first step is the solvation of the ketone by two acid molecules leading to the formation of two strong hydrogen bonds (I). An aromatic compound attacks the protonated carbonyl, and at a given moment, only one proton is transferred to carbonyl and forms a σ-intermediate component (II), while the other proton forms a hydrogen bonding with the carbonyl. In order to recover the aromaticity, the σ-intermediate loses a proton and forms a carbinol intermediate. This step is considered the rate-determining step for high molecular weight linear polymers.[128] Subsequently, the carbinol intermediate is solvated by three acid molecules (III), which facilitate the heterolytic cleavage of the C-O bond. This leads to the formation of the carbocation (IV) and water molecules as a by-product. Next, the carbocation reacts with another aromatic component to complete the cycle by generating the diaryl derivatives. The second step has a higher rate constant than the first step. The rate constants of the first (k_1) and the second (k_2) steps are crucial for generating high molecular weight polymer.[133] The ratio k_1/k_2 depends on three factors; the strength acidity, the electrophilicity of carbonyl compounds, and the nucleophilicity of the aromatic component. This means that k_1/k_2 can be tuned by modifying the reaction conditions or the monomer structure. The most commonly used acid is TFSA which is 10^3 times stronger than sulphuric acid and creates a convenient environment to generate super-electrophilic compounds.[130] TFSA is also responsible for recovering the aromaticity of the intermediate component by deprotonating the aromatic species. The acidity can be tuned by adjusting the ratio between acid and solvent (DCM), or acid and a carbonyl group. The increase of the acid strength of the environment decrease k_1 at the expense of the protonation energy and leaves k_2 unchanged.[130] The electrophilicity of the carbonyl group affects both the kinetics (e.g., activation energy) and the thermodynamics (e.g., the energy difference between the reactants and the final product) of the reaction. Electron withdrawing substituents such as -CF_3 attached to the carbonyl decreases the activation energy of the σ-intermediate formation step (II), which increases the rate constant (k_1) drastically.[134] On the contrary, the electron-withdrawing substituent reduces the stability of the second carbon cation (V), increasing the activation energy of the second step and decreasing the rate constant of this step. It is worth mentioning that when the carbonyl component is too electrophilic, when both vicinal sides have attached -CF_3, the activation energy of the second step is increased significantly, leading to reduced reaction rate to a level that is considered nonreactive.[133] On the other hand, when both adjacent sides of the carbonyl are tethered with electron donating groups, –CH_3, the activation energy of the first step is seven times higher than the activation energy of the second step, leading to unreactive species and no progress on the reaction.[133] Therefore, in order to generate a linear polymer with high molecular weight, the activation energy for both steps should not be very different, and the activation energy of the first step should always be higher, making the first step the rate-determining step. Additionally, an excess of the carbonyl component is added to increase the activation energy of the first step, significantly enhancing the overall polymerization rate and generating polymers with high

molecular weight.[130] Notably, a significant excess of the carbonyl results in side reactions and generates crosslinking products.[133] The nucleophilicity of the aromatic component is another factor that affects the rate constants of the polyhydroxyalkylation reaction. A less nucleophilic component, such as diphenyl, not only decreases the $k_{1,}$ but also decreases the k_2 with respect to the $k_{1,}$ due to the destabilization of the carbon cation (V), leading to an increase in the reaction time.[133] To conclude, the strength of acidity, the electrophilicity of the carbonyl component, and the nucleophilicity of an aromatic component are principal factors affecting the kinetics of superacid-mediated polycondensation reactions. Adjusting these factors allows for control of the reactivity of the monomers and obtain ether-free high molecular weight polymers.

2.2.2 Atom transfer radical polymerization

Free radical polymerization has been employed to polymerize vinyl monomers to produce a homopolymers and statistical copolymers.[135] It is used extensively on the industrial scale because it generates a wide range of polymers, is insensitive to monomer and reagent impurities, and possesses facile copolymerization conditions. The polymerization is very simple and consists of three essential steps. In the initiation step, an initiator molecule such as Azobisisobutyronitrile (AIBN) is thermally decomposed to generate two radicals to start the polymeric chain (Figure 17a). The propagation step allows the chain growth; the monomers are continuously added to the polymeric chain. The last step is the termination step and involves the termination of the growing chain. Termination of the polymeric chain can occur in two ways, by combination, where the chain ends combine with each other and generates a long polymeric chain, or by disproportionation, where a radical abstracts a hydrogen from another radical to produce two different ˝dead˝ polymer chains (Figure 17c). This can lead to polymers with broad molecular weight distribution, and difficulties to control the molecular weight or polymer architecture. The need and interest to synthesize polymeric structures with well-controlled molecular weight distribution and polymer architecture have been an attractive research topic for many polymeric groups during the twentieth century. Introducing the concept of controlled/living radical polymerization (CLRP opens a new area for polymer science.[136] It enables the researcher to synthesize polymeric architectures with different topologies, such as block, graft, and star, with well-defined polymer structure and molecular weight. Many controlled radical polymerization methods has been developed, such as Nitroxide-mediated radical polymerization (NMRP), reversible addition-fragmentation chain transfer (RAFT), and atom transfer radical polymerization (ATRP).[137] These techniques possess advantages and disadvantages regarding the reaction temperature, monomer scale, and initiator type. Among them, ATRP is the most common and well-established method for carbon-carbon bond formation because of the availability of a broad-scale initiator, adaptability to a higher number of monomers, high tolerance to many functional groups such as allyl,

hydroxyl, amino as well as the simplicity in experiment.[138] ATRP also provides a precise control over molecular weight,

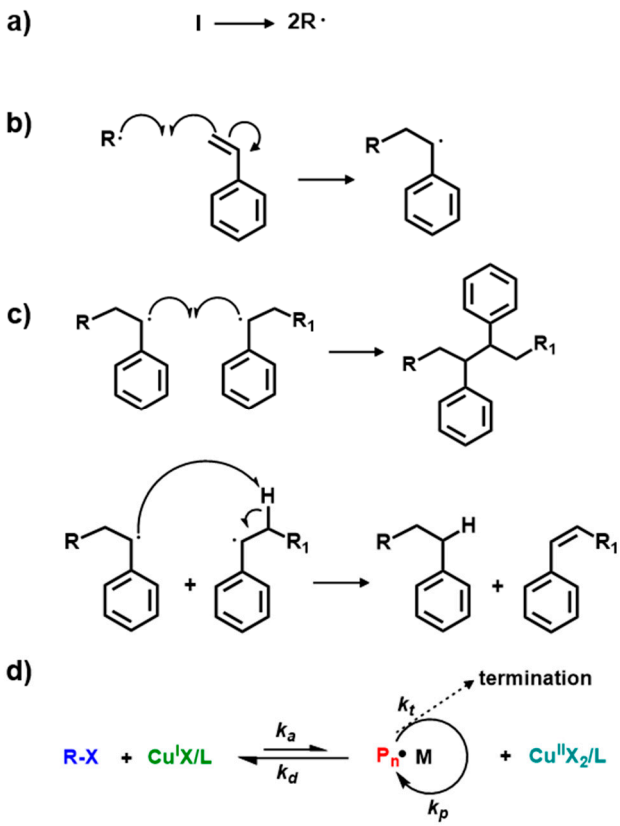

Figure 17. The overall reaction mechanism of the radical polymerization a) initiation, b) propagation, and c) termination. The conventional ATRP mechanism (d), where L and X represent ligand and halogen, respectively.[139]

molecular weight distribution, and chain end-functionality.[138] Traditional ATRP requires a low-oxidation state transition metal complex (CuX/L, X = Cl or Br and L = ligand), alkyl halide initiator (RX), and the monomer. Initially, CuX/L abstracts a halogen with a rate constant of activation (k_{act}) and forms a radical and oxidized species. Subsequently, the radical reacts with unsaturated monomer and generate an intermediate species. The intermediate species reacts quickly with a high oxidized metal complex with a rate constant of deactivation (k_{deact}) to abstract the halogen and generate the dormant alkyl halide species and a low-oxidation metal complex (Figure 17d). In order to control the architecture and the molecular weight of the polymer, the concentration of dormant species should be high and the concentration of the actively-propagating radicals should be low since both mitigate the termination reaction. Therefore, the equilibrium reaction should be shifted towards

dormant species.[138] The most commonly used transition metal is copper, mainly due to its low cost and versatility. The role of the ligand is to solubilize the metal ion, which also affects the reduction potential of the transition metal ion.[140] Alkyl bromides and chlorides are usually used as initiators.[141]

2.3 Post modification

2.3.1 Functionalization with tertiary amines

The quaternary ammonium groups in the polymer electrolyte, which are used as cationic groups and counter ions for OH^- anions, were introduced via S_N2 reaction between tertiary amine and an alkyl halide,[142] Figure 18.

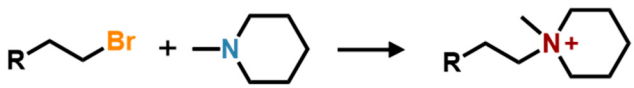

Figure 18. Menshutkin reaction, quaternization of a piperdine

These types of reactions, are straightforward and known as Menshutkin reactions. Additionally, these reactions are run in aprotic polar solvents such as NMP or DMSO to enhance the solubility of the reactant and product.[143] The reactions are usually run in the absence of a catalyst. Hence, to increase the efficiency and rate of the reactions, the tertiary amine is added in excess, around 4 equivalents to the alkyl halides. When dual quaternary groups such as bis-piperidinium, are introduced, the possibility of crosslinking and loop formation is increased, and both these reactions influence the IEC value and morphology of the membrane. Therefore, to mitigate crosslinking and loop formation, the tertiary bis–piperidinium groups were added in a considerable excess, around 10 equivalents to the alkyl halides, and the concentration of the reactant was kept very low.[74]

2.3.2 Cycloquaternization

The cycloquaternization refers specifically to the functionalization of a secondary piperdine group with alkyl halides and α,ω-dibromopentane to give mono- and spirocyclic quaternary ammonium cationic groups, respectively (Figure 19). Different from quaternization of tertiary amines, additional

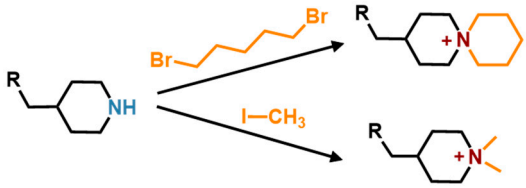

Figure 19. Cycloquaternization reaction of secondary piperdine with alkyl halides.

catalysts such as K_2CO_3 or DIPEA were required to complete the quaternization process. The former was employed to react to secondary amines with alkyl halides such as MeI. The latter was an efficient base used as a catalyst to synthesize spirocyclic quaternary ammonium from the secondary cyclic amines. DIPEA cannot be applied as a catalyst for synthesizing monocyclic quaternary cationic groups because it reacts with MeI and forms N,N-diisopropylethylmethylammonium iodide as a solid product.[143] The spirocyclic quaternizatio takes place in two essential steps. The first step is known as the intermolecular step and is related to the reaction between the secondary amine and α,ω-dibromoalkanes to form a tertiary amine. The second step, the intramolecular step, is connected with the reaction of the tertiary amine with an alkyl halide to form the spirocyclic ring. During the second step, side reactions such as branching and crosslinking may occur. Therefore, to avoid branching/crosslinking side reactions, the reaction is run under dilute conditions. The solution concentration plays an essential role in the reaction rate of the first and second step, i.e., in dilute conditions, the rate of the intermolecular step decreases while the rate of the intramolecular remains intact. Furthermore, the solvent is another factor that significantly influences the branching/crosslinking reactions because it is responsible for both dissolving all the compounds and maintaining the homogeneity of the mixture during the reaction. For example, if the mixture is inhomogeneous due to reactant precipitation, this leads to an increase in the local concentration and favors the intermolecular step, which facilitates crosslinking formation.[116] In order to support the homogeneity, a mixture of solvents can be applied; for example, in Paper IV and V, a DMSO and NMP mixture was used in the quaternization of the secondary amine.

2.4. Characterization methods

2.4.1. Polymer characterization

Nuclear magnetic Spectroscopy

Nuclear magnetic resonance (NMR) spectroscopy spectra were used to analyze and verify the chemical structure of both synthesized monomers and polymers. Bruker DRX400 model spectrometer and solvents such as DMSO-d_6 (δ = 2.5 ppm) and $CDCl_3$ (δ = 7.26) were employed for the analysis. Moreover, a small amount of TFA was added to the functionalized polymer in DMSO-d_6. The addition of TFA not only enhanced the dissolution of these polymers but also shifted the water peak downfield region. Hence, the signals that overlapped with the water signal were revealed.

Size –exclusion chromatography

Size-exclusion chromatography (SEC) is a technique employed to characterize the number average molecular weight (M_n) weight average molecular weight, (M_w) as well as polydispersity ($Đ_M$) of the precursor polymer. This technique is based on chromatography, a laboratory technique used to separate the mixtures. It consists of mobile and stationary phases; both have significant roles in the separation of a mixture based on different partitioning between the two phases. SEC separates the molecules of the polymer based on their hydrodynamic size. In the SEC, the column is the stationary phase and is made of small particles with different pore sizes. The mobile phase is the polymer solution, and when the polymer solution passes through the column, small polymer molecules spend more time inside the pores, leading to an increase in the time needed to pass the column. On the other hand, the large molecules spend less time in the column. The mass distribution of the precursor polymer was calculated using the conventional calibration method. The signal from the refractive index detector, a concentration-dependent detector, is recorded as a function of retention volume. The molar mass distribution was calculated by comparing the elution time with the calibration curve. In this work, two GPC instruments were used, the first being a Malvern Viscotek instrument with a 2×PL-Gel Mix-B LS column with a length of 30 cm equipped with OmniSEC Triple Detectors (refractive index, viscosity, and light scattering), and chloroform was used as eluent at 35 °C. A polystyrene standard with M_n = 96 kDa and PDI = 1.03 (Polymer Laboratories Ltd., Agilent Technologies and Water Associates) was used for calibration. The second instrument was an OMNISEC from Malvern, equipped with one TGuard, Org Guard Col 10×4.6 mm guard column, and two analytical columns 2×T6000M, General mixed Org.300×8.0 mm produced from Viscotek. Refractive index (RI) was used as a detector (Viscotek model 250). The conventional calibration was performed employing 6 polystyrene standard samples (M_n = 96 kDa and PDI = 1.03, M_n = 52.4 kDa and PDI = 1.02, M_n = 30 kDa and

PDI = 1.06, and M_n = 3 kDa and PDI = 1.03 , Polymer Laboratories Ltd., Agilent Technologies and Water Associates, M_n = 17.5 kDa and PDI = 1.06, M_n = 3500 kDa and PDI = 1.03, Polysciences. Inc. Warrington, PA 18976). The precursor polymer was dissolved in chloroform 24 h before the measurement and passed through a polytetrafluoroethylene filter with a pore diameter of 0.2 μm before injection.

Intrinsic viscosity

Intrinsic viscosity is an alternative method employed to estimate the molecular weight of the polymers that could not be dissolved in chloroform. The polymer was dissolved in DMSO and LiBr was added to prevent the polyelectrolyte effect. An Ubbelohde viscometer instrument was employed to measure the viscosity of the polymer solution and the blank solution at a constant temperature, 30°C. The elution time of the blank (0.1 M LiBr in DMSO) and the polymer solution at different concentrations (C) was used to calculate the inherent and reduced viscosity according to the equation below:

$$\eta_{\text{inh}} = \frac{ln\left(\frac{t_{\text{sample}}}{t_{\text{blank}}}\right)}{C} \quad (5)$$

$$\eta_{\text{red}} = \frac{\frac{t_{\text{sample}}}{t_{\text{blank}}} - 1}{C} \quad (6)$$

The two viscosities were plotted against concentration and linear regressions were performed. The intrinsic viscosity was determined as the average intersection of the linear regression of η_{inh} and η_{red} with the y-axis.

Thermogravimetric analysis (TGA)

Thermogravimetric analysis (TGA) was employed to investigate the thermal stability of the precursor polymers and the quaternized polymers in the Br^- form. All samples were analyzed employing a TA instrument Q500 at a constant heating rate of 10°C min^{-1} under a nitrogen atmosphere, and the change in the weight of the sample was monitored as a function of temperature. The sample was preheated at 150 °C and kept isothermal for 10 to 20 minutes to remove impurities such as water and solvent residuals before each measurement. The weight was evaluated during heating from 50 to 600 °C at 10 °C min^{-1}, and the decomposition temperature ($T_{d,95}$), at 5 % weight loss, was noted.

Differential scanning calorimetry (DSC)

Differential scanning calorimetry (DSC) is a thermo-analytical technique employed to observe the heat effects associated with phase transitions. This technique monitors the difference in heat flow between the sample and a reference at the same temperature and is presented as a function of temperature. The reference is an empty

alumina pan, and the sample is sealed in a similar alumina pan. All measurements shown in this thesis were performed under a nitrogen atmosphere employing Q2000 DSC from TA Instrument. Three cycles, heating-cooling-heating were applied for each sample. The first heating cycle is crucial in the DSC measurement because it deletes the thermal history of the sample, which may influence the results. The upper temperature for the heating-cooling-heating cycle in DSC is decided by the decomposition temperature ($T_{d,95}$, onset) measured using TGA and should be set 20-30 °C lower than $T_{d,95}$, onset.

2.4.2. Membrane preparation and characterization

Membrane preparation

All quaternized polymers in this work were cast into membranes from 5 wt% polymers dissolved in NMP or in a mixture of DMSO: NMP with a volume ratio of 1:1 at 80 °C for 48 h. First, a 5 wt % of the polymer solution was prepared at room temperature. The solution was subsequently passed through a Teflon filter with a pore size of 5 µm to a Petri dish (Ø = 5 cm) and transfered to a well-ventilated casting oven. After casting, deionized water was added, and the membrane was carefully peeled from the petri dish. The membrane was washed several times with deionized water and stored in water for 48 h before any characterizations.

Ion-exchange capacity (IEC)

The ion exchange capacity is an essential property of the anion exchange membrane because it not only directly affects the water uptake, but also the ion conductivity properties. IEC values show the number of the cationic group in milliequivalent per dry mass of a polymeric membrane (mequiv. g^{-1}), measured by ^{1}H NMR spectroscopy (theoretical value) and titration methods (experimental value). There are different titration methods such as acid-base titration and Mohr Titration. The former is not very recommended because the OH^- counter ions of the cationic groups can react with CO_2 and influence the results. In the latter, the membrane is in the Br^- form, which eliminates CO_2 contamination. This leads to more accurate results. The membrane is titrated in the Br^- form and is calculated according to the equation below.

$$IEC_{\mathrm{OH}} = \frac{IEC_{\mathrm{Br}}}{1-\frac{IEC_{\mathrm{Br}} \times (M_{\mathrm{Br}^-} - M_{\mathrm{OH}^-})}{1000}} = \frac{IEC_{Br}}{1-0.0629\, IEC_{Br}} \qquad (7)$$

In the present work, a membrane in the Br^- form (~0.05 g) was weighed immediately after drying at 50 °C for 48 h under a vacuum. Next, the membrane was placed in 0.2 M aq. $NaNO_3$ solution and kept at 40-50 °C for 7 days to complete the ion exchange. Subsequently, 5 ml of the solution with exchanged Br ion was titrated with 0.01 M aq. $AgNO_3$ in the presence of indicator potassium chromate (K_2CrO_4).

The endpoint was determined when the red-brown color appeared due to the formation of silver chromate (Ag_2CrO_4) precipitation. The titration is performed four times to mitigate random errors.

Water uptake

The presence of water in the membrane is crucial because water is not only responsible for the formation of interconnected ionic channels but is also used as ionic carriers, hence facilitating ionic transportation from one electrode to another during fuel cell operation. On the other hand, an excess of water compromises the membrane's mechanical properties and decreases the ionic conductivity due to dilution effects. Water uptake is affected by both IEC values and temperature. The latter is influences the thermal motion of water molecules and thus increases the water uptake at high temperatures. The procedure used to evaluate the water uptake is described below. At least 0.04 g of a membrane in Br^- form was dried at 50 °C for 48 h under vacuum. Next, the membrane was weighed, to determine the dry weight (W_{OH}-). The membrane was subsequently immersed in 1 M aq. NaOH, that prepared degassed water, and left under a nitrogen atmosphere inside of a desiccator at room temperature. The solution was changed at least three times with fresh 1 M aq. NaOH for 48 h and washed gently with fresh degassed water until the final pH of the washing water neutralizes to pH~7. Next, the membrane was transferred to a round bottom flask filled with degassed water, and the water uptake was measured at different temperatures, such as 20, 40, 60, and 80 °C, under a nitrogen atmosphere. Finally, the membrane was wiped gently with tissue paper and weighed quickly to determine the wet weight W'_{OH^-}. The water uptake was calculated as:

$$WU = \frac{W'_{OH^-} - W_{OH^-}}{W_{OH^-}} \times 100\% \qquad (8).$$

Small-angle X-ray Scattering

Small-angle X-ray scattering (SAXS) is an analytical technique used to study the morphology of material structures such as polymers, surfactants, and proteins.[144] Compared to other scientific equipment used to collect information at the nanoscale level, SAXS possesses many advantages. Firstly, the SAXS measurement does not require any extensive sample preparation. Additionally, the characterization can be carried out by using a small sample amount and can be applied in both liquid and solid states.[145] The morphology of the functionalized polymers provides vital information, i.e., the phase separation of the membrane which is essential for high ionic conductivity and low water uptake. SAXS records elastic scattering of X-rays at very low angles, typically 0.1 to 10°. Figure 20 shows an X-ray generator providing a monochromatic X-ray beam directed towards the sample. Most X-rays pass through the sample without interacting and form a primary beam. However, due to inhomogeneities in the sample, some X-rays are elastically scattered, which creates an angular distribution of the X-ray beams when they reach the detector.

This angular distribution contains information about the shape and size of the microstructures in the sample, as well as characteristic separation lengths between ordered structures.

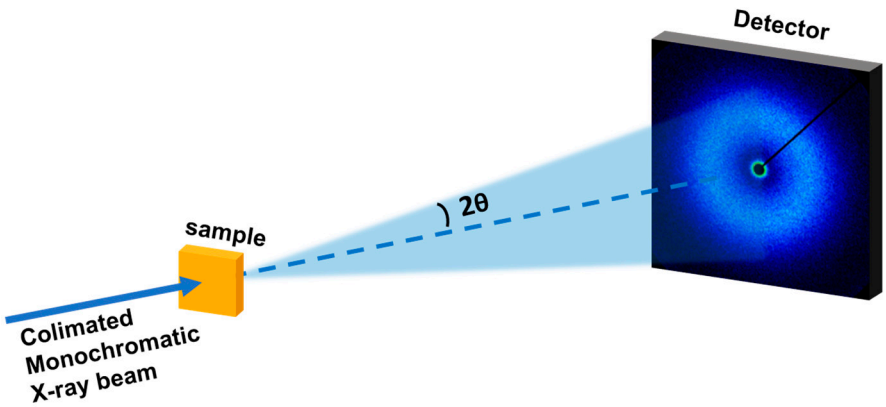

Figure 20. Illustration of a SAXS instrument with a scattering angle at 2θ by the sample.

In a typical experiment, the sample is irradiated with a collimated beam of monochromatic X-rays with a well-defined wave vector. Depending on the electron density, all atoms in the sample scatter the radiation in all spatial variations with different intensities. The higher the contrast in electron density, the higher the intensity of the scattered radiation. Then, the scattered radiation is recorded on the other side using a 2D detector, which detects scattering at small angles (2θ < 10°) (Figure 20).

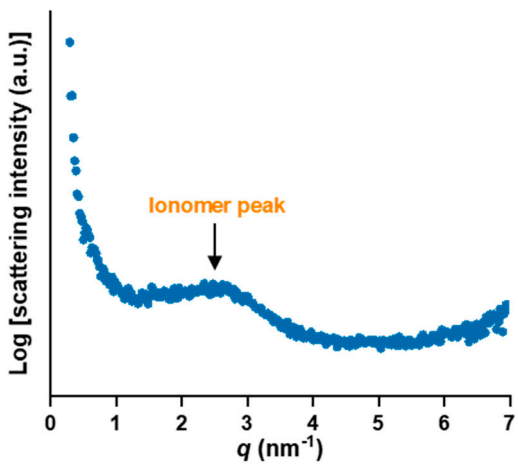

Figure 21. Scattering profile of an AEM with a clear visible ionomer peak

The recorded intensity is plotted as a function of the scattering vector (q), which is related to the scattering angle and can be calculated as:

$$q = \frac{4\,\pi\,sin\theta}{\lambda} \qquad (9),$$

where λ *is* the wavelength of the x-rays (usually 0.0154 nm for copper K_a x-ray source). The characteristic separation (d) of the ionomer peak (Figure 21), which presents the average of the distance between clusters, is calculated using Bragg's law:

$$d = \frac{2\pi}{q_{max}} \qquad (10).$$

All the SAXS data presented in this thesis were obtained from a SAXSLAB SAXS Instrument from JJ X-ray A/S, Denmark, in the q-ranges of 0.12-8 nm^{-1} by employing Cu K_a radiation (λ = 0.01542 nm).

Atom force microscopy

Atom force microscopy (AFM) is a high-resolution scanning microscope technique employed for measuring and imaging all types of surfaces, including polymers, ceramics, and composites. AFM works by generating images by physically scanning the surface sample by pushing the cantilever with a very sharp tip against the sample. As the tip approaches the surface, forces such as van der Waals, electrostatic and magnetic forces between the atoms in the

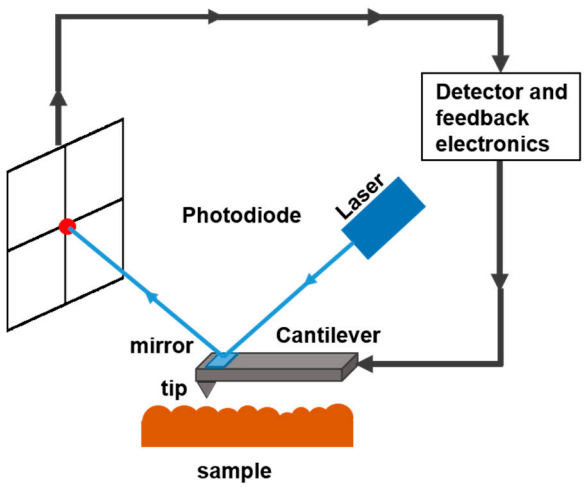

Figure 22. Schematic illustration of the AFM instrument.

sample will cause the tip to bend toward the sample surface (Figure 22). However, as the cantilever tip approached even closer to the sample surface, it triggered an increase in the repulsive forces, leading to the cantilever bending away from the

sample surface. The bending position (vibrating) of the cantilever is recorded with the help of a laser beam. The laser beam is reflected by a mirror positioned on top of the cantilever. As the cantilever bends, the beam is reflected in a different direction toward the photodiode detector. The detector collects all the changes and, with the help of a computer, can generate 3-D images of the sample morphology. Contact AFM and non-contact AFM are two methods employed to obtain images by AFM. In the former method, the cantilever moves across the sample, and the cantilever tip touches the sample's surface.[146] Touching the surface generates strong attractive and repulsive forces leading to the cantilever bending as it passes over the sample's surface. It is a simple method; however, touching the surface of the sample may cause significant damage to both the sample and the cantilever tip. In the latter method, the cantilever oscillates just above the surface and does not touch the surface. Here, in order to keep the cantilever from crashing into the surface, a precise high-speed feedback loop was used. This method protects the sample from damage, prolongs the cantilever tip's lifetime, and reduces the total operating cost.[147]

The AFM images recorded in this thesis were obtained using a Bruker Icon Atomic Force Microscope instrument. The tapping mode analysis of the air facing side of the membrane was analyzed by scanning 1 μm × 1 μm areas at a scan rate of 0.498 Hz.

Hydroxide Conductivity

The hydroxide conductivity of membranes in a fully hydrated state was determined by electrochemical impedance spectroscopy (EIS). The electrical impedance (Z) of the membranes was evaluated by applying a small amplitude of voltage as a function of frequency and measuring the current signal.[148] The impedance is defined as the ratio between voltage, V(t), and current, I(t), both are sinusoidal functions:.

$$V(t) = V_0 \cos(\omega t) \quad (11),$$

$$I(t) = I_0 \cos(\omega t + \varphi) \quad (12),$$

$$Z = \frac{V(t)}{I(t)} = \frac{V_0 \cos(\omega t)}{I_0 \cos(\omega t + \varphi)} \quad (13).$$

The $\omega = 2\pi f$ and φ is the angle shifted between the curves of voltage and current vs. time. When φ = 0, which means there is no phase shift, Equation 11 becomes identical to Ohm's law (V = IR). The conductivity depends on both the area and the distance between two the electrodes and was calculated according to the following equation:

$$\sigma = \frac{l}{AxR} \quad (14),$$

where A corresponds to the right-angle cross-sectional to the membrane and *l* is the distance between two electrodes. The conductivity of the membrane was plotted as

a function of frequency, and the value on the plateau region was taken as the hydroxide conductivity (Figure 23).

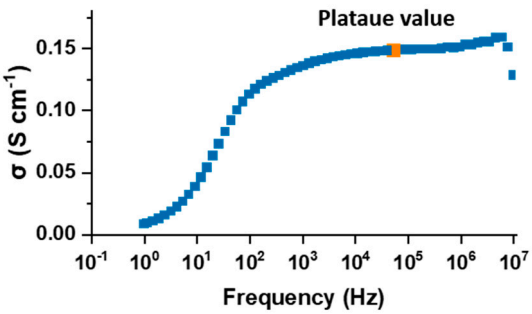

Figure 23. Hydroxide conductivity of the membrane as a function frequency at a constant temperature and a plateau value

The hydroxide ion conductivity of the membranes was characterized by using a Novocontrol high-resolution dielectric analyzer V 1.01S with a voltage amplitude of 50 mV at a range of frequency from 10^0 to 10^7 Hz. First, the samples were immersed in degassed 1 M aq. NaOH to exchange anions into OH^- form, carefully washing with water until the pH reached neutral, finally and stored under nitrogen for 24 h. The membrane was sandwiched between two stainless steel electrodes, as shown in Figure 24.

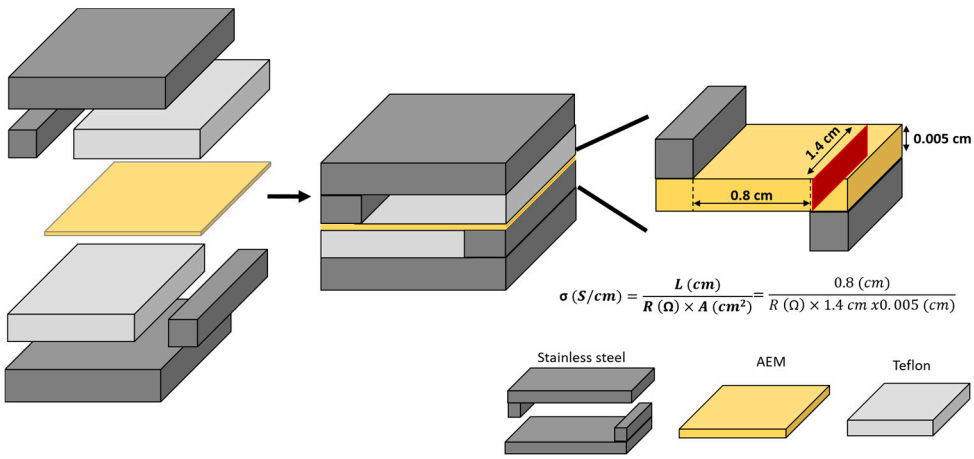

Figure 24. The two-probe cell assembly employed in-plane OH^- conductivity measurement of the AEM under fully hydrated conditions.

The cell assembly should be done as quick as possible to reduce CO_2 contamination. Subsequently, the OH^- conductivity was characterized during the cycle 20→80→20→80 ºC under fully hydrated conditions using a two-probe method.

Alkaline stability

Chemical resistance of the membranes under harsh conditions at elevated temperatures is a vital characteristic for a membrane to be employed in the fuel cell application The alkaline stability of the membrane was evaluated by standard analytical techniques such as NMR spectroscopy, UV-spectroscopy, FT-IR, and FT-Raman spectroscopy to analyze the compound's chemical structure before and after alkaline treatment. Among these tools, NMR spectroscopy is the most widespread technique because it supports quantitative analysis and provides detailed information about the degradation products after alkaline treatment. In this work, all alkaline stability characterization was performed employing ^{1}H NMR spectroscopy. The alkaline stability of the membrane was determined at different concentrations of the base, i.e., 2, 5, 7, and 10 M aq. NaOH, at storage time from one week to several weeks, and at temperature 90 and 120 °C. The chemical degradation of the membrane was evaluated by comparing the integrals of new peaks that emerged after the alkaline treatment with that of the aromatic peaks which were stable during the alkaline treatment. Comparison of these peaks made it possible not only to calculate the degradation percentage but also to unravel the chemical degradation pathways. Below is described in detail the procedure for alkaline stability characterization. A thick glass pressure tube, an inner Teflon tube, and a safety seal were used for the alkaline treatment (Figure 25).

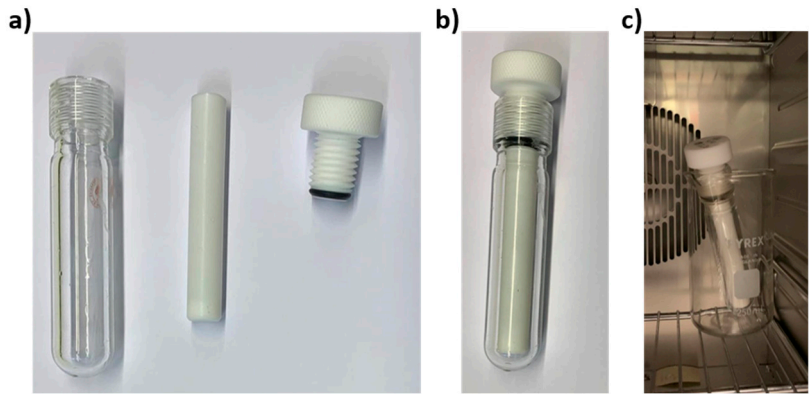

Figure 25. Equipment used for the alkaline treatment, a) thick pressure sustainable glass tube, home-made Teflon inner tube, and a screw lid, b) the assembled holder, and c) the set up positioned in an oven.

Firstly, a Teflon made inner tube was placed into the glass pressure tube. Next, a piece of a membrane (~20 mg) and 10 ml concentrated NaOH solution was transferred to the inner tube. Subsequently, the glassy tube was closed carefully with the screw lid. The Teflon inner tube prevents the corrosion of the thick pressure glass tube by the very corrosive basic solution. Furthermore, the screw lid prevents water evaporation and maintains the concentration of the basic solution, and the temperature constant

during the alkaline treatment. An oven is employed to keep the temperature stable. After the alkaline treatment, the membrane was washed with deionized water several times to remove the low molecular weight products formed during degradation and then immersed into 1 M aq. NaBr solution to complete the ion exchange from OH^- to Br^- form for 2 days. During this time, the NaBr solution was exchanged more than three times. The membrane sample was then dried at room temperature for 48 h, dissolved in DMSO-d_6, and characterized with the ^{1}H NMR spectrometer.

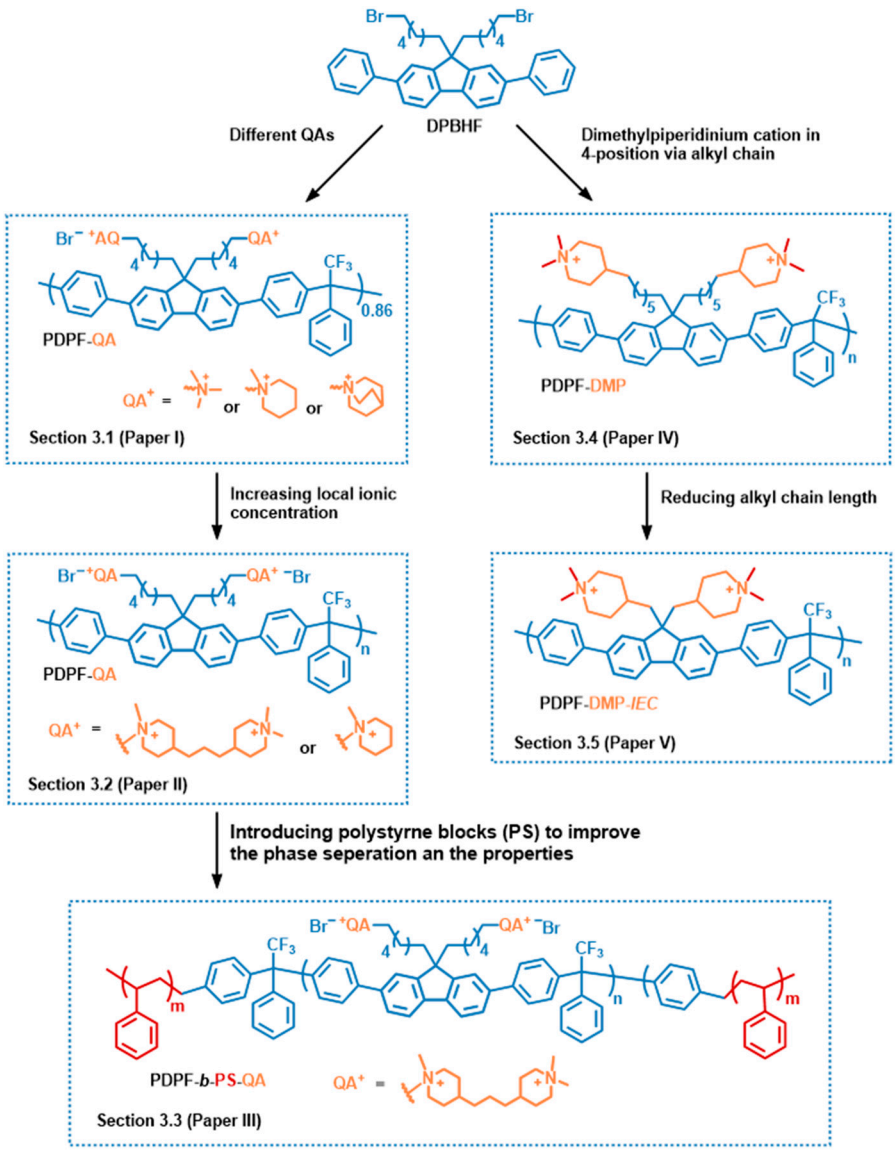

Figure 26. Polymeric structure of AEMs presented in the section 3.1-3.5.

Summary of appended papers

This chapter is based on the result and discussion of each article included in this thesis. The chapter is divided into five parts, each part represents one article. Each part will begin with short motivation explaining the polymer architecture, followed by the essential aspects of the monomer and polymer synthesis, and finally a discussion of membrane properties.

3.1 Ether-free fluorene-based anion exchange membranes and the effect of different cationic groups

The motivation behind the first paper is related to three aspects: synthesizing an ether-free polymer backbone, introducing cationic groups via an alkyl spacer, and exploring the effect of the different quaternary ammonium groups. A polymer with heteroatoms in the backbone has often been seen to be chemically unstable in alkaline environment. Therefore, ether-free polymer backbones based on polyaromatics and polyolefins have been reported to be alkali-stable polymer backbones. One of the most facile ways to synthesize aryl ether-free polymer backbone is via acid-mediated Friedel-Crafts polycondensation reactions. These types of reactions are also known as polyhydroxyalkylation reactions. A series of three anion exchange membranes based on the same polymer backbone functionalized with Qui, Pip, and TMA cation were successfully synthesized, as shown in Figure 27. The fluorene-based monomers were used as an electron-rich arenes domain in this work due to many advantages. Fluorene has an excellent rigid tricyclic planar structure; two six-membered phenyl rings are attached on each side of the five-membered ring system. Additionally, the tricyclic structure allows modification and introduction of different functional groups. For instance, the two acidic protons in the five-membered ring are very reactive in the presence of a base and can be used to tether two bromo-alkyl chains. Other positions that can be utilized to produce different fluorene derivatives are the 2 and 7 positions (e.g., the addition of extra six-membered rings via Suzuki coupling). Moreover, fluorene possesses outstanding chemical and thermal properties. Lastly, fluorene is less expensive (100 g per $60) compared to *p*-terphenyl (100 g per $141) and is widely available. Two fluorene-based monomers (DPBHF and DODPF) were synthesized by alkylation reactions followed by Suzuki coupling reactions.

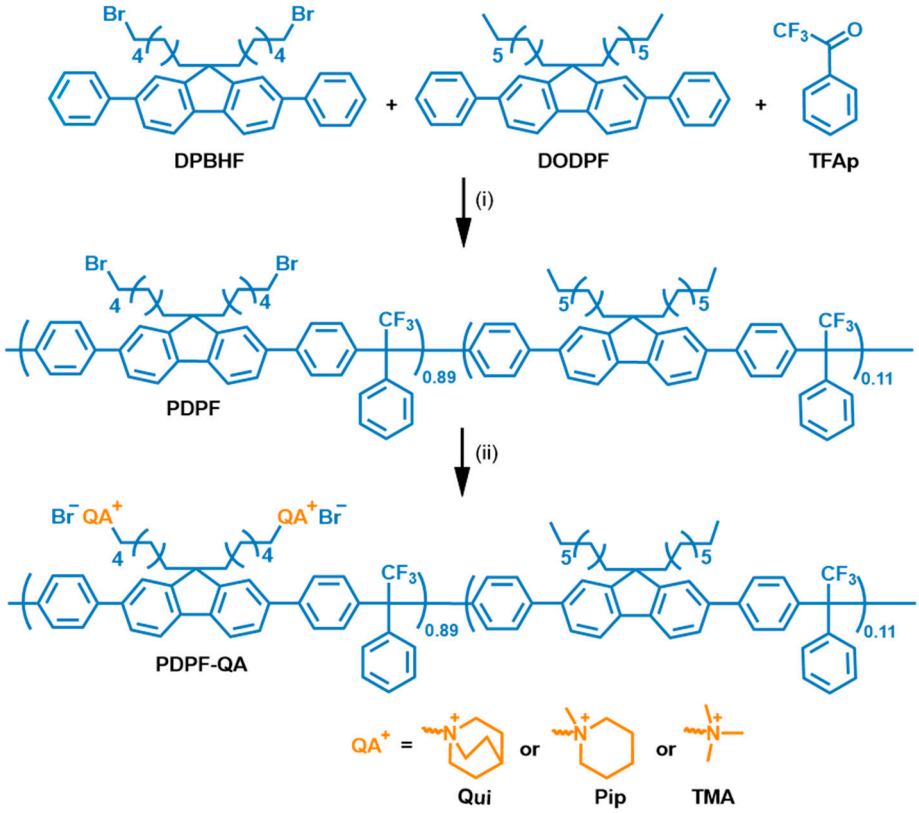

Figure 27 The synthetic pathway to PDPF copolymers functionalized with QAs in 2 steps: superacid-mediated polyhydroxyalkylation reactions (i) and quaternization reactions of Qui, Pip, and TMA cation (ii), respectively.

The DPBHF monomer contains two flexible bromohexyl chains, which were used to introduce the QA cations. It has been reported that the alkyl spacer between the polymer backbone and cationic group enhances both the ionic conductivity and the alkaline stability of the cationic group. Additionally, two flexible octyl chains were tethered to DODPF to enhance the solubility of the precursor and the final polymer, and also to control the IEC values. The diphenylfluorene monomer derivatives possess a more rigid structure than the non-phenylated ones. This facilitated the polyhydroxyalkylation reaction and provided polymers with higher chain rigidity, which reduces the water uptake and swelling of the AEMs. The electron-withdrawing group (-CF_3) attached to the carbonyl group in the 2,2,2-trifluoroacetophenone (TFAp) made the polycondensation reaction possible and promoted the reaction selectivity to obtain a linear and high molecular weight polymer. The fluorine atom incorporated into the polymer backbone increased the polymer's solubility, glass transition temperature (T_g), chemical stability, and thermal stability. The precursor polymer was synthesized by superacid-mediated

polyhydroxyalkylation of DPBHF, DODPF, and TFAp and denoted as PDPF. The bromohexyl chains of precursor copolymer were then reacted with a tertiary amine to produce PDPF-Qui, PDPF-Pip, and PDPF-TMA, respectively. All the polymers were cast into transparent and mechanically flexible membranes.

Water uptake and OH^- conductivity of fully hydrated AEMs were measured as a function of temperature. Figure 28 shows that the water uptake increased with temperature and IEC.

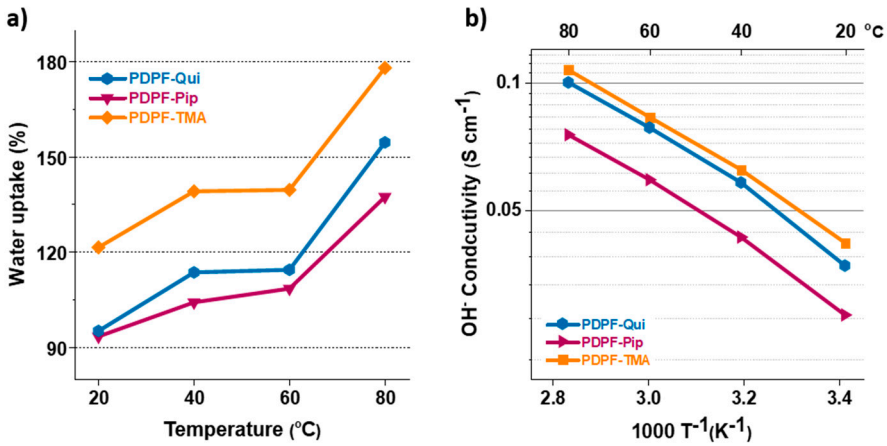

Figure 28. The water uptake of AEMs in the OH^- form at 20-80 °C (a) and OH^- conductivity of AEMs as a funtiontion of T^{-1} obtained under fully hydrated conditions (b).

The water uptake of PDPF-TMA, with the highest IEC, increased from 121% at 20 °C to 178% at 80 °C. The water uptake of the AEMs with similar IEC values, PDPF-Qui and PDPF-Pip, reached 95 and 93%, respectively, at 20 °C. However, at 80 °C, the water uptake of PDPF-Qui was higher and reached 154%, compared to the water uptake of PDPF-Pip, which reached 137%. The OH^- conductivity of the AEMs increased with temperature and followed the water uptake trend of the AEMs. At 80 °C, the OH^- conductivity of the PDPF-TMA, PDPF-Qui, and PDPF-Pip reached 107, 100, and 75 mS cm^{-1}, respectively.

The thermal decomposition temperature ($T_{d,95}$) of the AEMs in the Br^- form was studied by TGA under nitrogen atmosphere. As seen in Table 1, the PDPF-Qui showed the highest thermal stability with $T_{d,95}$ = 267 °C, while PDPF-Pip and PDPF-TMA possessed similar thermal stability with almost the same $T_{d,95}$ = 200 and 203 °C, respectively. The high decomposition temperature of the PDPF-Qui can be explained by the cage-like and symmetrical structure of the Qui cation.

Table 1 Properties of the AEMs.

AEM	IEC (mequiv g^{-1})		WU_{80}[c] (wt%)	σ_{OH}[c] (mS cm^{-1})	$T_{d,95}$[d] (°C)
	theoretical[a]	titrated[b]			
PDPF-Qui	1.78 (2.01)	1.77 (1.99)	154	100	267
PDPF-Pip	1.82 (2.06)	1.80 (2.03)	137	75	200
PDPF-TMA	1.96 (2.24)	1.95 (2.22)	178	107	203

[a]Calculated from the ^{1}H NMR spectra in the Br^- form (IEC in the OH^- form within parentheses).

[b]Calculated from titration in the Br^- form (IEC in the OH^- form within parentheses).

[c]Measured at 80 °C in the OH^- form in the fully hydrated state.

[d]Measured by TGA under nitrogen atmosphere at 10 °C min^{-1}

Alkaline stability is another critical feature of the AEMs since it directly affects OH^- conductivity, performance, and durability of the AEMs and limits their application in the fuel cell. ^{1}H NMR spectroscopy was employed to evaluate and investigate the alkaline stability of the AEMs. The ^{1}H NMR spectra were recorded and compared before and after alkaline treatment, in 2 M aq. NaOH at 90 °C for 672 h, and in 5 M aq. NaOH at 90 °C for 168 h. The reason behind the addition of TFA before any ^{1}H NMR characterization was to shift the water peak above 10 ppm, and to protonate any tertiary amines which could form after alkaline treatment. After alkaline treatment, new signals emerged in the region 4.5-5.8 ppm and around ~9 ppm, while the aromatic signals did not change, as shown in Figure 29a-c. To reveal the degradation pathway, the region around the new signals was expanded and is presented in Figure 28d-f. The intensity and the position of the new peaks between 4.5 and 5.8 ppm indicated the existence of vinylic protons, most probably formed via Hofmann elimination reactions. As seen in Figure 29d-f, in all the samples, the intensity and position of the peaks at ~4.7 and ~5.5 ppm (*p* and *o*) corresponded to the alkene ($–CH_2$) and alkenyl ($–CH=CH_2$) protons, respectively, formed via Hofmann elimination in the alkyl chain. In addition, PDPF-Pip possessed another vinylic signal that emerged at ~4.9 (*r*) and ~5.7 ppm (*k*), corresponding to Hofmann elimination in the Pip ring, leading to ring opening and forming a protonated tertiary amine at 9.2 ppm (*y*). No second set of vinylic signals was detected for PDPF-Qui, demonstrating that the cage-like bicyclic configuration of Qui cation was highly resistant to Hofmann elimination. In addition, the new signals emerging at ~9 ppm corresponded to protonated tertiary amines, created during alkaline treatment via ring-opening Hofmann elimination (PDPF-Qui and PDPF-Pip) or nucleophilic substitution (PDPF-Pip and PDPF-TMA).

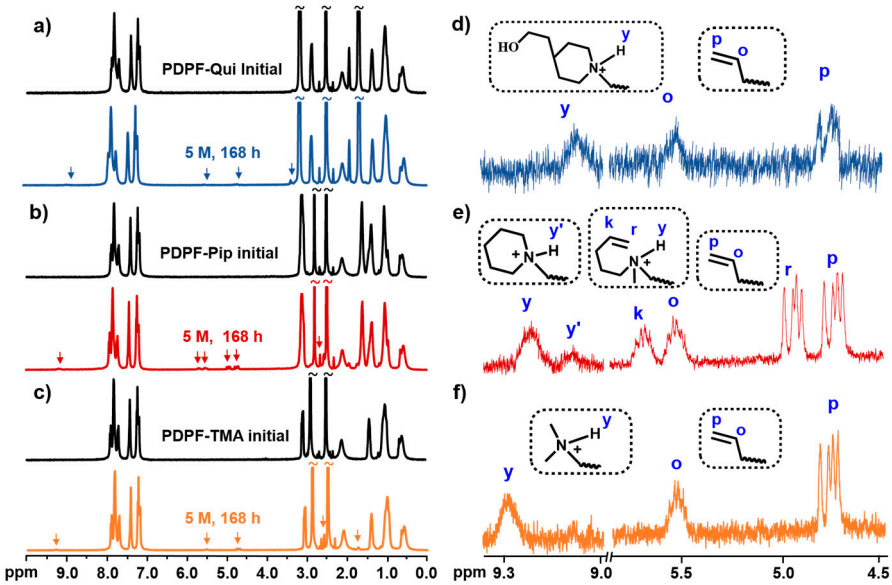

Figure 29. [1]H NMR spectra of PDPF-Qui (a), PDPF-Pip (b), and PdPF-TMA (d) were recorded in DMSO-d_6/TFA before and after alkaline treatment with 5 M aq. NaOH at 90 °C for 168 h. The new signals appeared between 4.5-5.8 and 9.0-9.4 ppm after alkaline treatment, 5 M, aq. NaOH at 90 °C for 168 h were indicated by arrows and expended in (d), (e), and (f) panels for PDPF-Qui, PDPF-Pip, and PDPF-TMA, respectively.

The degree of ionic loss of each degradation mechanism was calculated using [1]H NMR data by comparing the integrals of the newly emerged signals to that of the aromatic signals. As can be seen in Table 2, PDPF-Qui possessed the highest stability after storage in 5 M aq. NaOH at 90 °C for 168 h with a total ionic loss of merely ~5%. PDPF-Pip showed the lowest stability at the same condition, with a total ionic loss of ~23%. It is essential to mention that even if the number of the β-hydrogen protons in the ring was twice of the β-hydrogen protons in the alkyl spacer, the β-protons in the alkyl spacer were almost 4 times more vulnerable to OH^- attack. The higher stability of β-protons in the ring was related to the ring configuration, which increased the activation energy of the transition state of Hofmann elimination.

Table 2. The ionic loss of the AEMs calculated from [1]H NMR data after alkaline treatment.

Alkaline treatment	AEM	Ionic loss by Hofmann elimination [a] (%)		Ionic loss by nucleophilic substitution [b] (%)	Total ionic loss (%)
		alkyl spacer	alicyclic ring		
2 M aq. NaOH, 90 °C, 672 h	PDPF-TMA	4.4	n.a.	4.4	8.8
	PDPF-Pip	7.7	4.0	0.5	12.2
	PDPF-Qui	1.2	0	3.0	4.2
5 M aq. NaOH 90 °C, 168 h	PDPF-TMA	4.4	n.a.	4.4	8.8
	PDPF-Pip	11	5.0	7.2	23.2
	PDPF-Qui	1.6	0	3.2	4.8

[a] Hofmann elimination in both alkyl spacer and alicyclic rings. [b] Nucleophilic substitution at an α-carbon leading to methyl or ring-opening substitution (n.a. = not applicable).

To conclude, the ether-free fluorene-based copolymers tethered with TMA, Pip, and Qui cations, respectively, via hexyl spacers were successfully synthesized. Among them, the membrane with Qui cations possessed the highest thermal and alkaline stability with good OH^- conductivity. The high chemical stability of the Qui cation can be attributed to the bicyclic structure, which imposes the configuration restrictions that contribute to increasing the transition state energy of the Hofmann elimination reaction. Finally, no degradation signal was detected from the ether-free polymer backbone in the ^{1}H NMR spectra, indicating high chemical stability.

3.2 Effect of the local ionic concentration

This section discusses the effect of local ionic concentration on the overall properties of AEMs. Four ether-free fluorene-based copolymers tethered with dual bis-piperidinium (bis-Pip) and mono-piperindium (Pip) cationic groups via alkyl chains were successfully synthesized. The introduction of the dual piperidine rings via the alkyl chains was expected to affect the morphology of the membrane by facilitating the formation of ionic clusters and to enhance ionic conductivity and alkaline stability. The effect of the content of bisPip cations was investigated in terms of water uptake, OH^- conductivity, and thermal and chemical stability.

Four ether-free fluorene-based precursor copolymers were synthesized from diphenylbis(6-bromohexyl)fluorene (DPBHF), dimethyldiphenylfluorene (DMDPF), and trifluoroacetophenone (TFAp) monomers via a superacid-mediated polyhydroxyalkylation reactions, and denoted as PDPF-Br-*x*. The *x* represents the degree of bromination (DB), and was adjusted by controlling the DPBHF: DMDPF ratio in the monomer feed since both monomers have similar reactivities. The molecular weight, polydispersity ($Đ_M$), glass transition temperature (T_g), and thermal decomposition temperature ($T_{d,95}$) of the precursor polymer were measured and are shown in Table 3. As can be seen in Table 3, the T_g increased from 240 to 278 °C as the DB decreased from 81% to 40%.

Table 3. Properties of the PDPF-Br-x precursor copolymers.

Copolymers	DB[a] (%)	Mn[b] (kg/mol-1)	$Đ_M$ [b]	T_g [c] (°C)	$T_{d,95}$ [d] (°C)
PDPF-Br-81	81	95	2.8	240	360
PDPF-Br-71	71	44	1.7	240	383
PDPF-Br-53	53	40	3.3	263	384
PDPF-Br-40	40	35	2.0	278	383

[a] Calculated by ^{1}H NMR spectroscopy. [b] Evaluated by SEC. [c] Measured by DSC. [d] Analyzed by TGA under N_2.

Three precursor polymers were functionalized with bisPip cations and this was achieved by two consecutive Menshutkin reactions. The first Menshutkin reaction

is critical because it may cause crosslinking or loop formation. These potential side reactions reduce the final IEC and affect the morphology of the AEM. Therefore, a significant excess of 4,4'-trimethylenebis(1-methylpiperidinine) was added dropwise to a dilute precursor polymer solution. The second Menshutkin reaction was successfully completed with methyl iodide. The cationic copolymers were denoted as PDPF-bisPip-*y*, where *y* indicates the final IEC in the OH^- form. In addition, the functionalization of PDPF-Br-81 with mono-piperidinium cation was also achieved via a Menshutkin reaction with N-methyl piperidine. The cationic copolymer was named PDPF-Pip-y, where y denotes the final IEC in the OH^- form.

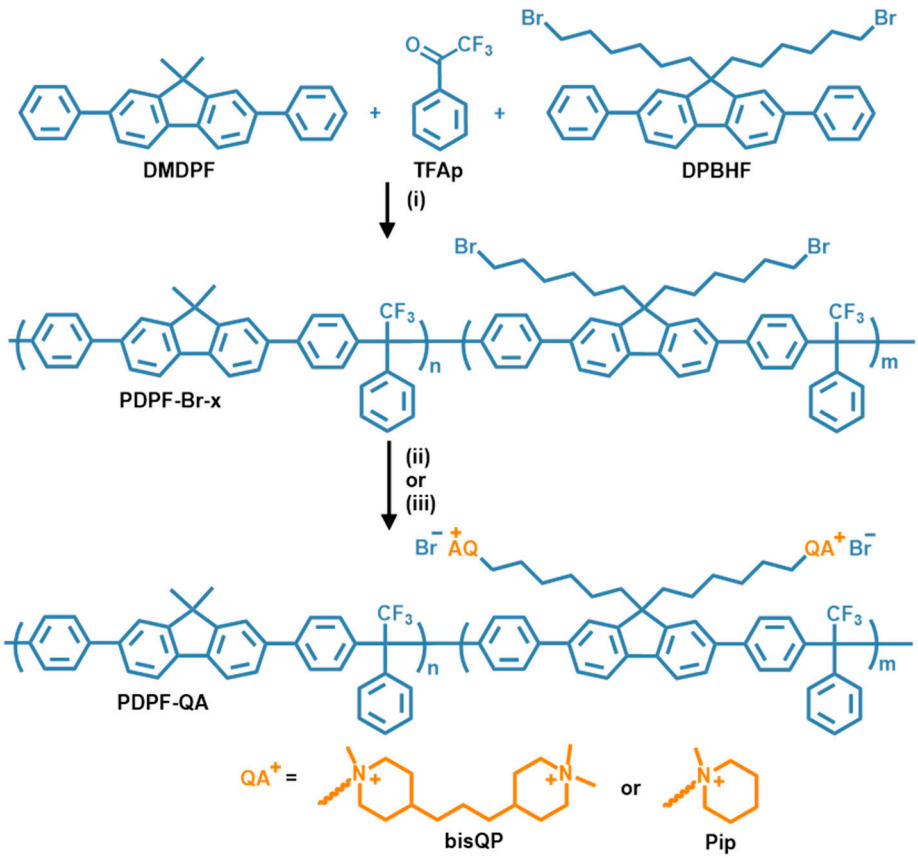

Figure 30. Synthesis of the precursor and quaternized copolymers in three steps: superacid-mediated polycondensation reaction (i), attachment of the bisPip cationic groups in two consecutive Menshutkin reactions (ii), attachment of mono-piperidinium cation via Menshutkin reaction (iii).

The water uptake and hydroxide conductivity of fully hydrated AEMs in the OH^- form were analyzed between 20 and 80 °C, and the results are presented in Figure 31. The water uptake of the AEMs increased with IEC and temperature. PDPF-

bisPip-2.8, with the highest IEC, showed a water uptake of 329 and 556% at 20 and 80 °C, respectively. Moreover, the local ionic concentration promoted the formation of the large water-rich domain, leading to increased water uptake (Figure 31a). For example, at similar IEC values, PDPF-bisPip-2.0 showed higher water uptake than PDPF-Pip-2.0. Figure 31b showed that increasing the IEC values increased the hydroxide conductivity of the AEMs. In addition, the high local ionic concentration enhanced the ionic conductivity. For example, at the same IEC value, PDPF-bisPip-2.0 with four piperidinium cations per fluorene unit and PDPF-Pip-2.0 with two cations per fluorene showed OH^- conductivities of 85 and 75 mS cm^{-1}, respectively, at 80 °C.

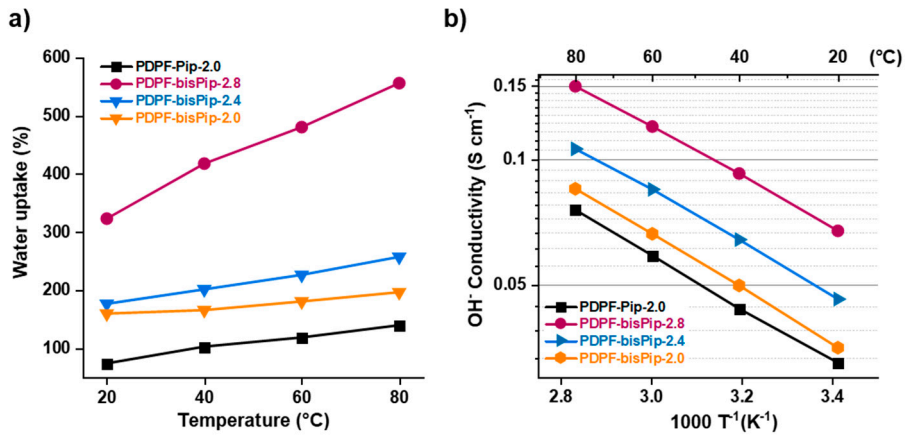

Figure 31. Water uptake of fully hydrated AEMs in hydroxide form as funtion of temperature (a) and OH^- conductivty of fully hydrated AEMs as a function of T^{-1}.

The alkaline stability of the AEMs was evaluated by analyzing changes in ^1H NMR spectra before and after alkaline treatment. The AEMs were immersed in 2 M and 5 M aq. NaOH for 672 and 168 h, respectively, at 90 °C. After the alkaline treatment, the AEMs were washed several times with fresh water to remove any low molecular weight by-product formed during the treatment, and the AEMs were then ion-exchanged with 1 M aq. NaBr . Figure 32a-b shows the ^1H NMR spectra of AEMs, before and after storage in 5 M aq. NaOH for 168 h at 90 °C. No new peaks emerged in the aromatic region, indicating again the outstanding alkaline stability of the fluorene-based polymer backbone. On the other hand, new peaks appeared in the region 4.5-5.7 ppm and 8.8-9.3 ppm suggesting degradation of the piperidinium cations. For four AEMs, the intensity and position of the new peaks at 4.5-5.7 ppm indicated the presence of two sets of vinylic protons (Figure 32e-h). The first set emerged at ~4.7 (*o*) and ~5.4 (*p*) ppm and was attributed to the Hofmann elimination in the alkyl chain. The second set appeared at ~4.9 (*r*), 5.5 ppm (*k*), formed from Hofmann elimination in the Pip ring. Moreover, for four AEMs, the signal detected

in the region 8.8-9.3 ppm was suggested to be the protonated tertiary amine formed due to Pip-ring opening Hofmann elimination. From the ^{1}H NMR spectra of four AEMs, detecting any new signal corresponding to degradation via nucleophilic substitution was not possible.

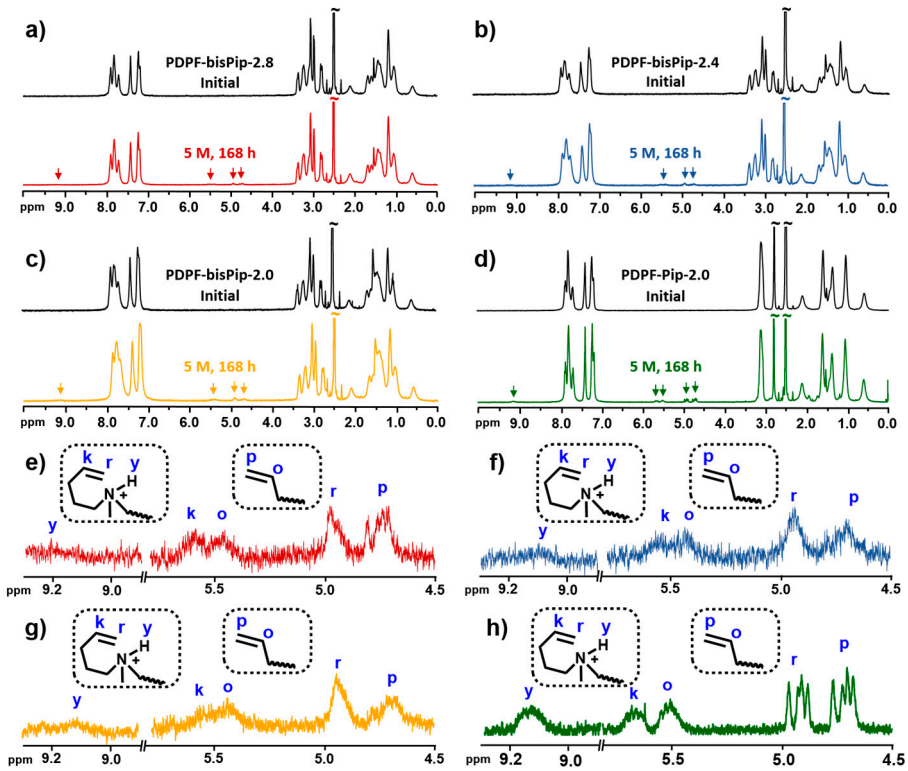

Figure 32. ^{1}H NMR spectra before and after alkaline tratment in 5 M, aq. NaOH during 168 h at 90 °C of a) PDPF-bisPip-2.8, b) PDPF-bisPip-2.4 (c) PDPF-bisPip-2.0 and d) PDPF-Pip-2.0. The signals emerged in the region 4.5-5.7 ppm and 8.8-9.3 ppm after storage in 5 M, aq. NaOH for 168 h at 90°C are amplified in e) PDPF-bisPip-2.8, f) PDPF-bisPip-2.4, g) PDPF-bisPip-2.0 and h) PDPF-Pip-2.0.

Furthermore, another alkaline treatment, 2 M aq. NaOH, 168 h at 120 °C was completed, and the ionic loss of each different alkaline treatment was evaluated by ^{1}H NMR spectroscopy and shown in Figure 33. The ionic loss by different degradation mechanisms was calculated by comparing the integrals of the aromatic region with the relevant signals. PDPF-bisPip-2.8 showed the highest alkaline stability after storage in the 5 M aq. NaOH, 168 h at 90 °C, with 4 and 2% ionic loss from Hofmann elimination in the alkyl spacer and Pip-ring, respectively. It is important to emphasize that even if the number of the β-hydrogens in two Pip rings is 4 times higher than for the β-hydrogens in the alkyl spacer, the β-hydrogens in the alkyl spacer were almost 8 times more prone to OH^{-} attack than those hydrogens

in the Pip-ring. The outstanding alkaline stability of the piperidinium ring is due to its ring structure. After harsh alkaline treatment, 2 M aq. NaOH, 168 h, at 120 °C, the degree of degradation of PDPF-bisPip-*x* series increased drastically, demonstrating the significant effect of temperature. PDPF-Pip-2.0, on the other hand, was impossible to analyze due to crosslink formation caused by amino alcoholates.

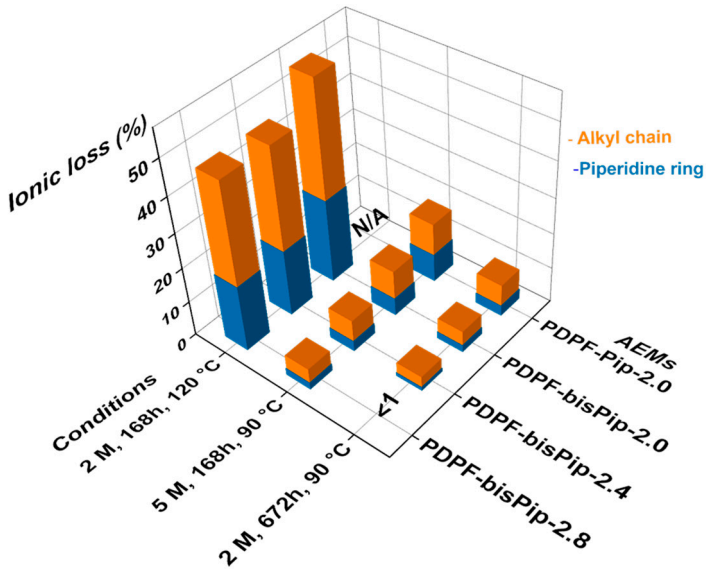

Figure 33. Ionic loss by Hofmann elimination of the AEMs, calculated from ^{1}H NMR spectra after different alkaline treatments (N/A: not analyzed due to insolubility).

To conclude, tethering two pairs of piperidinium cation via alkyl spacers to a polymer backbone increased the local ion concentrations and improved the properties of the membrane. The membranes with dual piperidinium cations produced higher ionic conductivity and better thermal and alkaline stability than mono piperidinium cations.

3.3 Effect of polystyrene blocks on the AEMs properties

In previous work (Paper II), four different ether-free random copolymers were synthesized using two diphenyl monomers (DPBHF and DMDPF) and TFAp via super acid-mediated polyhydroxyalkylation reactions. Subsequently, the random precursor copolymers were functionalized with dual piperdinium cations. The AEMs of the corresponding copolymers showed good thermal stability, but high water uptake values. This compromised the mechanical properties of the membrane and diluted the ionic concentration, which directly reduced the ionic conductivity. To improve the properties, the chemical structure and morphology of AEMs were modified by attaching two hydrophobic blocks (B) at each chain end of the polymer backbone to form BAB triblock copolymer with a central ionic (A) block. This synthetic approach was expected to further improve the mechanical properties, alkaline stability, and ionic conductivity of the membrane. Moreover, to investigate the effect of the length of the blocks and thus ionic content on the membrane properties, four different triblock copolymers with different B-block were synthesized.

Four BAB triblock copolymers with the same ether-free fluorene-based midblock (A) and with flanking polystyrene (B) of different lengths were synthesized according to Figure 34. The polymerization was carried out to obtain terminal benzyl groups at the polymer chain ends. Subsequently, the benzylic positions (end group) of the PDPF-Me precursor polymer were brominated with NBS to produce an ATRP macroinitiator (PDPF-Br) with a bromobenzyl at each chain end (Figure 34). ATRP was then performed to polymerize styrene to form the polystyrene block and give PDPF-*b*-PS-*x*, where *x* represents the wt % of the polystyrene blocks in the triblock copolymers, which was adjusted to provide the desired IEC. Finally, the bromohexyl chains in the midblock were functionalized so that each fluorene unit carried two pairs of dual piperidinium cations. Thus, the final PDPF-*b*-PS-bisPip-*IEC* series had midblock with a very high ionic content with and overall *IEC* = 2.0, 2.2, 2.4, and 2.6 mequiv. g^{-1}, respectively. These triblock polymers were dissolved in NMP and cast into AEMs at 80 °C for 48 h.

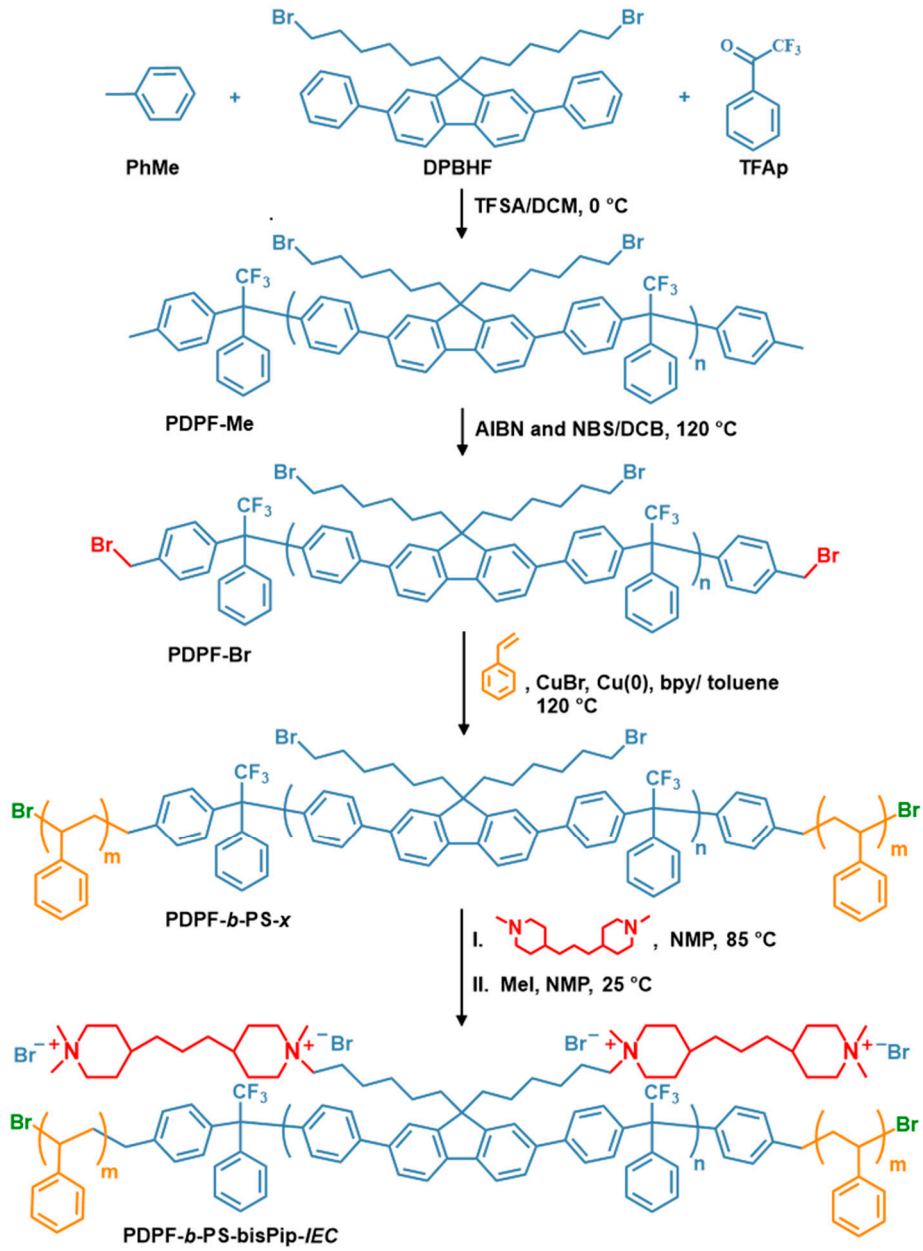

Figure 34. Preparation of the BAB triblock copolymers in four steps: superacid-mediated polyhydroxyalkylation reactions, followed by benzylbromination reaction to generate the macroinitiator. ATPR was then employed to synthesize the polystyrene block, and finally, the midblock was functionalized with dual piperidinium cations to give the PDPF-*b*-PS-bisPip-*IEC* series.

Atomic force microscopy (AFM) was used to study the surface morphology of triblock copolymer AEMs, with the resulting phase images shown in Figure 35. As

seen, the triblock copolymers clearly showed the expected nanoscale phase separation, where the dark areas represent the soft ionic phase and the bright areas indicate the hard hydrophobic phase domain. Moreover, the hard hydrophobic domains gradually increased with the polystyrene block content in the triblock polymers. For example, PDPF-*b*-PS-bisPip-2.0, which possessed the highest polystyrene block content, showed a more significant and obvious hydrophobic phase than PDPF-*b*-PS-bisPip-2.6, which has the lowest polystyrene concentration.

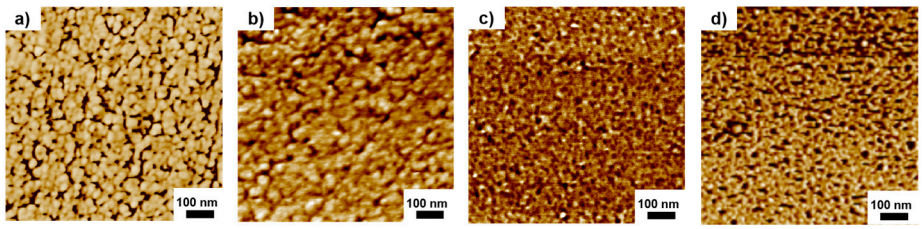

Figure 35. AFM phase images recorded on the membrane surfaces of PDPF-*b*-PS-bisPip-2.0 (a), PDPF-*b*-PS-bisPip-2.2 (b), PDPF-*b*-PS-bisPip-2.4 (c), and PDPF-*b*-PS-bisPip-2.6 (d) where the polystyrene block content decreased from a to d.

The water uptake of fully immersed AEMs in the OH^- form was gravimetrically determined and is shown in Figure 36. As expected, the water uptake increased with temperature and IEC. At 20 °C, the AEMs showed a water uptake between 70 and 324%, depending on the IEC values, and water uptake increased to between 123 and 528% as the temperature raised to 80 °C. When the water uptake of the PDPD-*b*-PS-bisPip-2.0 sample was compared to that of a corresponding fluorene-based random copolymer tethered with piperidinium cations (PDPF-bisPip-2.0 from the Paper II) at the same IEC value (2.0 mequiv. g^{-1}), the triblock copolymer showed around 40% less water uptake. The lower water uptake of the triblock copolymer sample may be attributed to the presence of the flanking B blocks of polystyrene, which were hydrophobic and in the glassy state which locked the ionic midblock in a physical network to restrict the water uptake. The OH^- conductivity followed the same trend as the water uptake and increased with temperature and IEC. For example, at 80 °C, the PDPF-*b*-PS-bisPip-2.6, with the highest IEC value, reached OH^- conductivity of 162 mS cm^{-1}, which was twice as the ionic conductivity of PDPF-*b*-PS-bisPip-2.0 (81 mS cm^{-1}). Moreover, the BAB triblock copolymers exhibited higher OH^- conductivity at the given IEC value than the corresponding random copolymers described in Paper II. This may also be attributed to the presence of the flanking polystyrene blocks, which supported the mechanical integrity, and the ionic midblock which generated water rich percolating channels and facilitated the transportation of the OH^- ions.

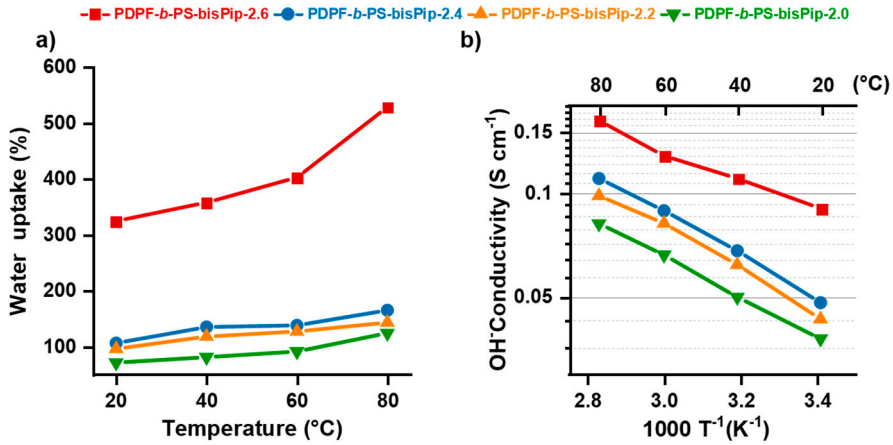

Figure 36. Water uptake of fully hydrated AEMs in the OH^- form as a function of temperature (a), and OH^- conductivity of fully immersed AEMs as a function of T^{-1} (b).

^{1}H NMR spectroscopy was used to analyze changes in the chemical structure of the current AEMs after alkaline treatment. The AEMs were immersed in 2 M and 5 M aq. NaOH for 672 and 168 h, respectively, at 90 °C. No new peaks were detected in the ^{1}H NMR spectra of all the AEMs after 672 h storage in 2 M aq. NaOH at 90 °C, indicating the excellent alkaline stability of the AEMs under harsh alkaline treatment. After 168 h storage in 5 M aq. NaOH at 90 °C, however, the AEMs were not completely soluble in the DMSO-d_6/TFA, and no data could be recorded. This may be because of the formation of amino alcoholates during the alkaline treatment, which may then react with the piperidine ring and generate ether-crosslinkers.

To conclude, the molecular design of BAB triblock copolymers with a center block densely tethered with piperidinium cations, flanked by non-ionic, glassy blocks, improved AEMs properties significantly in comparison with corresponding random copolymers. The polystyrene (B) blocks improved the mechanical properties and restricted the water uptake, while the fluorene-based ionic (A) blocks facilitated the ion conductivity, resulting in AEMs with very high alkaline stability and hydroxide conductivity.

3.4 Effect of tethered position of mono- and spirocyclic quaternary ammonium

Until now we have discussed the properties of the AEMs with piperidinium cations tethered to the polymer backbone in the 1(*N*)-position via alkyl chain employing Menshutkin reactions. Under alkaline treatment, it was demonstrated that the β-protons in the alkyl chain were more sensitive to Hofmann elimination than protons in the piperidinium ring (Figure 37a-b). However, if the piperidine-based cationic group is tethered *via* the 4-position (Figure 37c-d) to the polymer backbone, all the sensitive β-protons of the alkyl chain are removed. Additionally, the conformational freedom of the alicyclic ring increases the transition energy of the elimination step resulting in highly alkaline stable cations.

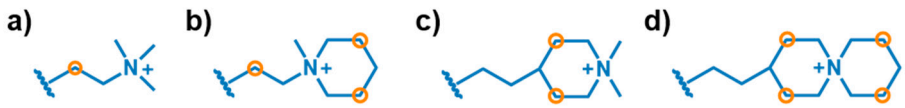

Figure 37. Ionic loss by Hofmann elimination of the AEMs, calculated from ^{1}H NMR spectra after different alkaline treatments (N/A: not analyzed due to insolubility).

Therefore, in the present work, we developed a novel polymer design in which the DMP and ASU cations were attached in 4-positions to the fluorene-based backbone via heptyl spacers (Figure 38). The impact of this novel architecture was investigated in terms of thermal and alkaline stability, water uptake and ion conductivity. Tethering the piperidine-based cations in the 4-position was the most challenging task in this work since there was a lack of both facile synthetic pathways and commercially available monomers. Alkyl-alkyl Suzuki coupling was first used to attach N-Boc-methyl piperidine to dibromoalkyted diphenyl fluorene (DPBHF) monomer, and the product was then treated with aq. HCl to remove the protecting group, Boc, and give DPF-PiH. The alkyl-alkyl Suzuki coupling reaction is rarely used in the synthesis because alkyl halides possess slow oxidative addition to Palladium, and facilitate the β-hydration elimination reaction. Therefore, to enhance the efficiency of the reaction, a bulky electron-rich phosphine ligands PCy_3, a catalyst $Pd(OAc)_2$, and a base $K_3PO_4{\cdot}H_2O$ were used as a catalyst system. Superacid-mediated polyhydroxyalkylation reaction was subsequently used to polymerize DPF-PiH with TFAp and generate the precursor homopolymer, PDPF-PiH (Figure 38).

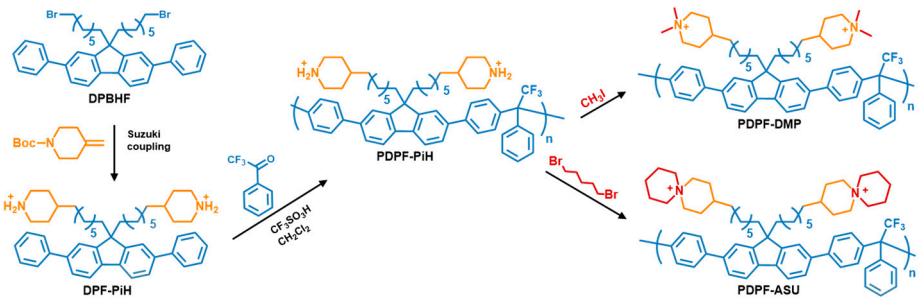

Figure 38. Synthetic pathway to generate quaternized PDPF-DMP and PDPF-ASU.

Phenylated fluorene provided a rigid backbone (PDPF) which facilitated film formation and improved the mechanical strength of the membrane. PDPF-PiH was then quaternized with methyl iodide and 1,5-dibromopentane, respectively, to produce the functionalized polymers PDPF-DMP and PDPF-ASU, respectively. To eliminate any potential branching/crosslinking side reactions,during the quaternization of PDPF-ASU, the PDPF-PiH was diluted and transferred dropwise to the diluted solution of 1,5-dibomopentane. The functionalized polymers were characterized in terms of water uptake, thermal and alkaline stability, and ionic conductivity, and the results are shown in Table 4.

Table 4. Properties of PDPF-DMP and PDPF-ASU

AEM	IECBr (mequiv. g-1)		IECOHa (mequiv. g-1)	WU80c (wt%)	λ80c	σ80c (mS cm−1)	Td,95 d (°C)
	Theoreticala	Titrated b					
PDPF-DMP	1.90	1.95	2.15	111	29	124	273
PDPF-ASU	1.76	1.62	1.98	45	12	76	332

[a] Calculated from the chemical structure of the polymers; [b] Determined by Mohr titrations; [c] Measured at 80 °C in hydroxide form, under fully hydrated conditions (immersed); [d] Measured by TGA under N_2 at 10 °C min^{-1}.

Table 4 shows that the water uptake of the PDPF-DMP was 2.5 times higher than PDPF-ASU, with a value of 111% and 45%, respectively, at 80 °C. The lower uptake of the PDPF-ASU can be attributed to the lower IEC and the bulky structure of the ASU cation. The OH^- conductivity of PDPF-DMP and PDPF-ASU reached 124 and 76 mS cm^{-1}, at 80 °C, respectively. The high conductivity of the former can be ascribed to the higher IEC value and water uptake; both may contribute to ionic clustering and the formation of percolating water domain channels, facilitating the ionic transport.

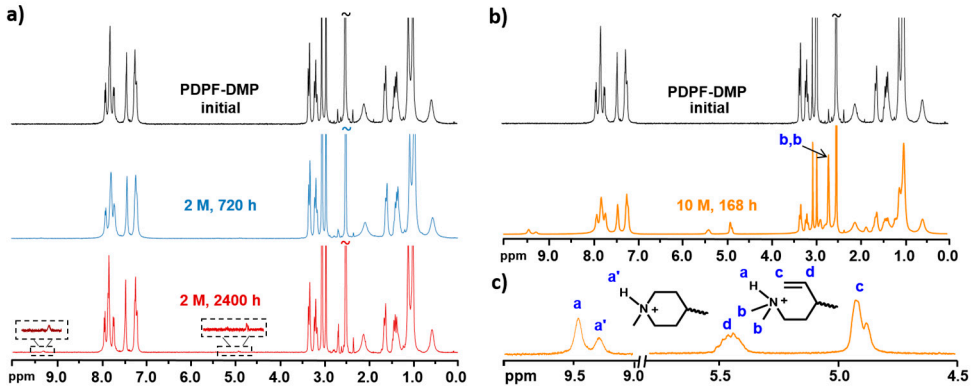

Figure 39. [1]H NMR spectra of PDPF-DMP a) before and after alkaline treatment, 2 M aq. NaOH, at 90°C, b) before and after storage in 10 M aq. NaOH, for 168 h, at 90 °C and c) the new signals emerging in the region 4.5-5.7 and 9.0-10 ppm after alkaline treatment 10 M, aq. NaOH, 168 h, at 90°C were expanded.

The alkaline stability of the AEMs was analyzed by storing membrane samples in 2, 5, 7, and 10 M aq. NaOH at 90 °C for different periods of time and the ^{1}H NMR spectra of the PDPF-DMP are shown in Figure 39. No change in the aromatic region of the ^{1}H NMR spectra was detected after alkaline treatment, indicating a high stability of the ether-free fluorene-based polymer backbone. In contrast, after storage in the 10 M aq. NaOH for 168 h, at 90 °C, new peaks emerged in the region of 4.5-5.7 and 9-10 ppm, which are magnified and shown in Figure 39c. Hofmann elimination and nucleophilic substitution are two main degradation pathways of the alicyclic DMP and ASU cations, and both pathways generate a tertiary amine as a by-product. The intensity and position of the peaks at ~4.7-5.3 ppm (*c* and *d*) indicate the formation of an alkene group (–CH=CH$_2$), suggesting Hofmann elimination in the ring. In addition, the two signals that emerged at ~9.2 ppm (*a*) and 9.3 ppm (*a'*) corresponded to protonated tertiary amines formed by nucleophilic substitution and Hofmann elimination, respectively (Figure 39c). Additionally, the quantitative ionic loss of each degradation mechanism was calculated after comparing the integrals of the new signals with the integrals of the aromatic signals, shown in Figure 40.

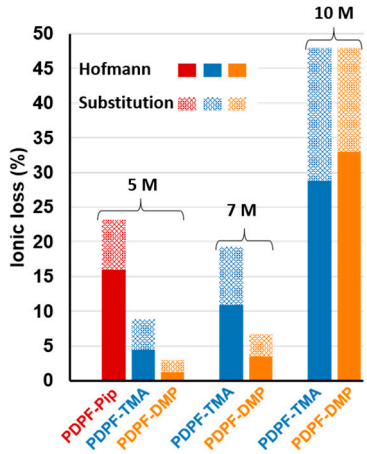

Figure 40 Ionic loss estimated from ^{1}H NMR spectra of PDPF-Pip, PDPF-TMA and PDPF-DMP via Hofmann elimination and nucleophilic substituiton, respectively.

The rate of degradation increased with alkaline concentration. At low alkaline concentrations 5 and 7 M aq. NaOH, 168 h, at 90 °C, PDPF-DMP was relatively stable with a total ionic loss <10%, and the nucleophilic substitution was the dominant degradation pathway. When the alkaline concentration was increased from 7 to 10 M, the total ionic loss increased drastically to 48%, and Hofmann elimination was the dominant degradation step. The positive effect on the alkaline stability by tethering via the 4-position is clearly shown in Figure 40. Piperidinium cations were tethered to the fluorene-based polymer via alkyl chains in the 1(*N*)-position and the 4-position to give PDPF-Pip and PDPF-DMP, respectively. After 168 h storage in 5 M aq. NaOH, 168 at 90 °C, the total ionic loss of PDPF-DMP and PDPF-Pip were only 3% and 23%, respectively. PDPF-DMP showed 8 times less ionic loss than PDPF-Pip, and the ionic loss via Hofmann elimination was reduced by 92% in PDPF-DMP. Moreover, PDPF-DMP membrane showed an outstanding alkaline stability, with a total ionic loss of < 8% after 2400 h storage in 2 M aq. NaOH, at 90 °C. Furthermore, PDPF-DMP showed a higher alkaline stability with less ionic loss than PDPF-TMA in 5 and 7 M aq. NaOH, and similar alkaline stability when the alkaline conditions increased to 10 M aq. NaOH.

PDPF-ASU showed traces of degradation after 720 h storage in 2 M aq. NaOH, 90 °C, and the solubility of PDPF-ASU decreased significantly with at increasing alkaline concentration and the treatment time. The solubility decreased due to the crosslinking via the degradation products formed during the alkaline treatment.

To conclude, a positive effect on ionic conductivity and alkaline stability was demonstrated by tethering the piperidinium cation via the 4-postion. In this novel molecular design, all the sensitive β-protons in the alkyl chain (from PDPF-Pip)

were replaced with β-protons in the alicyclic ring. The flexibility of the alkyl chain allows ring relaxation. This promotes a geometrical conformational freedom, which enhances the activation energy transition step in the elimination reaction, leading to a more stable cationic material.

3.5 The effect of alkyl spacers in the alicyclic quaternary ammonium anion exchange membranes

The polymer architectures shown in paper IV possessed a novel molecular structure with piperidinium-based cations attached via the 4-position and showed outstanding alkaline stability. A long and flexible alkyl chain with seven carbons was used to tether the cation group to the polymer backbone. It has been reported that the alkyl spacer chains with 4-6 carbons improve the phase separation, facilitate the formation of ionic clustering and percolation channel, and possibly enable fast ion transportation. However, long alkyl chains (>6 carbon) decreases the glass transition of the polymer leading to the softer polymeric materials. Additionally, in paper IV, the seven-carbon alkyl chain in the fluorene-based monomer increased the molecular weight of the repeating unit and restricted the IECs. Therefore, in this work, the piperidinium-based cations were attached to the 4-position on diphenylated fluorene monomers via direct S_N2 reaction. Using methyl bridges instead of the heptyl chain for tethering the cationic group decreased the molecular weight of the functionalized repeating unit, allowing higher IECs of the final product. TFAp, DPF-DHP, and DMDPF were polymerized via superacid-mediated polycondensation reactions to generate precursors PDPF-DHP-*x*, where *x* represents the percentage of the piperidinium containing fluorene unit (Figure 41). The precursor copolymers were then reacted with methyl iodide and 1,5-dibromopentane to give the PDPF-DMP-*IEC* series and PDPF-ASU-*IEC*, respectively. The impact of the methyl bridge was investigated in terms of morphology, water uptake, thermal and alkaline stability, and ionic conductivity.

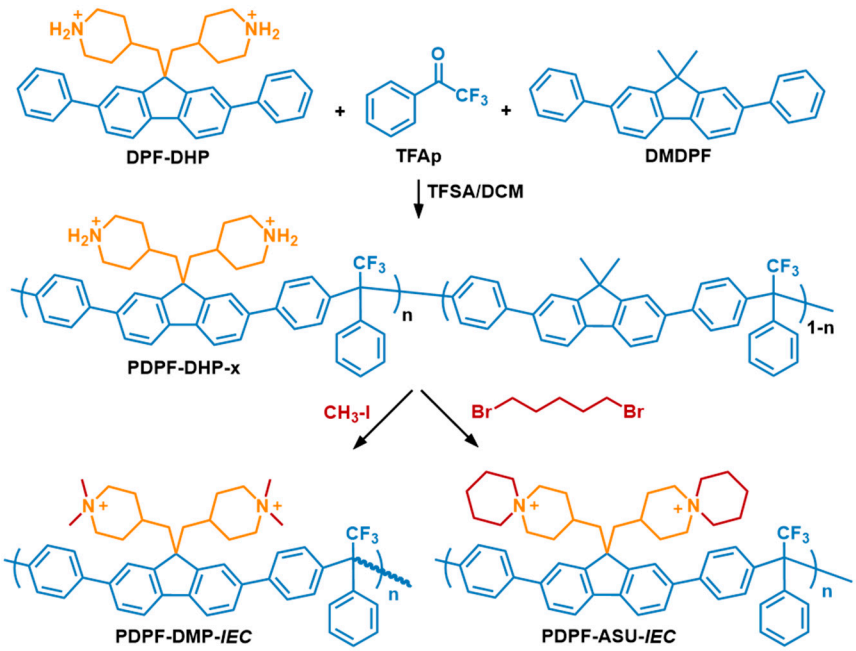

Figure 41. Synthetic pathways to the PDPF-DMP-*IEC* series of copolymers and and the PDPF-ASU-*IEC* homopolymer.

According to SAXS measurements, the introduction of piperidinium-based cations via methyl bridges was found to facilitate the phase separation of AEMs and provided distinct ionomer peaks (Figure 42). For the PDPF-DMP-*IEC* series, the characteristic distance (*d*) decreased as the IEC value increased. In addition, the structure of the cationic group affected the characteristic distance. For example, at similar IEC values, PDPF-DMP-2.4 and PDPF-ASU-2.4 showed *d* = 2.25 and 1.91 nm, respectively.

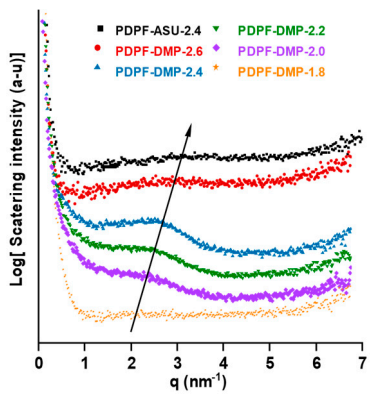

Figure 42 SAXS profile of PDPF-DMP-*IEC* series and PDPF-ASU-*IEC.*

Ionic clustering promotes the formation of percolating channel, leading to higher ionic conductivities. Water uptake and OH^- conductivities of the AEMs were measured and are shown in Table 5. The water uptake increased with the IEC for all the AEMs. At 80 °C, the water uptake of PDPF-DMP-1.8 was 3.4 times lower than PDPF-DMP-2.4, with values of 121 and 490%, respectively. AEMs with similar IEC values, PDPF-DMP-2.4 and PDPF-ASU-2.4, showed water uptake of 490 and 298 %, respectively, at 80 °C.

Table 5. Properties of the PDPF-DMP-*IEC* series and PDPF-ASU-*IEC*.

AEM	IEC (mequiv.g^{-1})		WU_{80}[b] (wt%)	λ[b]	σ_{OH}[b] (mS cm^{-1})	$T_{d,95}$[c] (°C)	d[d] (nm)	Ionic loss [e] (%)
	Theoretical a	Titrated						
PDPF-DMP-1.8	1.79 (1.61)	1.80 (1.61)	121	36	99	269	2.85	45
PDPF-DMP-2.0	2.00 (1.78)	2.06 (1.83)	134	36	115	246	2.54	35.3
PDPF-DMP-2.2	2.22 (1.94)	2.18 (1.93)	290	84	126	283	2.38	31.4
PDPF-DMP-2.4	2.39 (2.08)	2.46 (2.13)	490	111	153	282	2.25	29.9
PDPF-DMP-2.6	2.59 (2.25)	2.59 (2.23)	NA	NA	181	310	2.05	27
PDPF-DMP-ASU	2.38 (2.07)	2.41 (2.10)	298	64	140	335	1.92	N A

[a] Calculated from the chemical structure in the OH^- form (Br^- within parenthesis);[b] Measured at 80 °C in the OH^- form in the fully hydrated state; [c] Measured by TGA at 10 °C min^{-1} under N_2; [d] Analyzed by SAXS in the Br^- form; [e] Evaluated by ^{1}H NMR spectra after 168 h storage in 2 M, aq. NaOH, at 90 °C. (NA = not analyzed).

The lower water uptake of PDPF-ASU-2.4 can be attributed to the bulky structure of ASU. The OH^- conductivity of all the AEMs increased with IEC. At 80 °C, except for PDPF-DMP-1.8 which reached 99 mS cm^{-1}, all AEMs reached an ionic conductivity value above 100 mS cm^{-1}. The OH^- conductivity of the PDPF-DMP-2.6 was almost twice that of PDPF-DMP-1.8, with OH^- conductivity values of 185 and 99 mS cm^{-1}, respectively. AEMs with a similar IEC, PDPF-DMP-2.4 and PDPF-ASU-2.4, reached OH^- conductivities of 153 and 140 mS cm^{-1}, respectively. The lower ionic conductivity of the latter can be attributed to the bulky structure of the cationic group and insufficient water uptake to form percolating channels for OH^- ions.

The alkaline stability of the PDPF-DMP-*IEC* series and PDPF-ASU-*IEC* was investigated by ^{1}H NMR spectroscopy. The AEMs were stored for 30 days in 2 M aq. NaOH and for 168 h in 5, 7, and 10 M aq. NaOH at 90 °C. The structure change in the ^{1}H NMR spectra of AEMs before and after alkaline treatment allows the analysis of the degradation mechanisms pathway and the calculation of the ionic loss quantitatively. All AEMs showed outstanding alkaline stability with no degradation after storage in 2 and 5 M aq. NaOH at 90 °C for 720 h and 168 h, respectively.

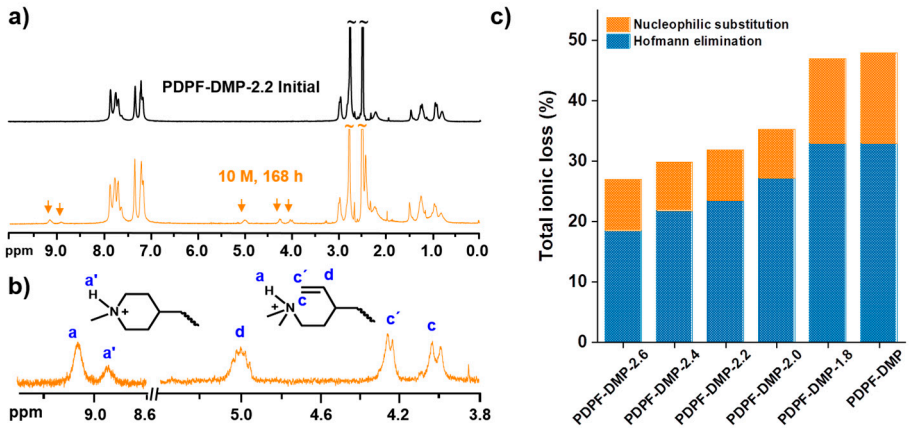

Figure 43. (a) Alkaline stability of the PDPF-DMP-2.2 membane after 168 h storage in 10 M aq. NaOH at 90°C, (b) expansion of the new signal emerged between 3.8-5.8 and 8.6-9.6 ppm , and (c) total ionic loss of the PDPF-DMP-*IEC* series and PDPF-DMP after alkaline treatment in 10 M, aq. NaOH for 168 h at 90°C.

Figure 43a shows the ^{1}H NMR spectrum of PDPF-DMP-2.2 after storage in 10 M aq. NaOH for 168 h at 90 °C, and news peaks emerging in 3.8-5.8 and 8.6-9.6 ppm, indicating the degradation of the piperidinium cationic group, were then expanded in Figure 43b. No change in the aromatic region of the ^{1}H NMR spectrum implied the outstanding alkaline stability of the backbone. The intensity and the position of the peaks at ~4.0 (*c*), and 4.2 (*c´*) ppm to the peak at ~5.0 (*d*) was 1:1:1: in ratio indicating the formation of vinylic protons, most probably by Hofmann elimination. Moreover, the peak intensity that emerged at 9.12 ppm (*a*) is similar to that at 4.0 ppm (*c*), indicating the tertiary amine formed by Hofmann elimination. The new peak at 8.9 ppm implied the tertiary amines formed by nucleophilic substitution. Additionally, the ionic loss via Hofmann elimination and nucleophilic substitution was calculated by comparing the intensity of the corresponding peaks with intensity of the aromatic peaks, as shown in Figure 43c. Hofmann elimination dominated the total ionic loss and decreased with increasing IEC of the membranes. All the present AEMs showed lower total ionic loss than PDPF-DMP, where the piperidine-based cations were attached via heptyl spacers. The methyl bridge provided and supported a geometric conformational freedom of the piperidine ring. This flexibility increased the activation energy of the elimination leading to a more alkaline stable piperidine-based cationic group. Moreover, the number of water molecules per OH^- group, the λ value, may also enhance the alkaline stability; the higher the λ value, the less aggressive the OH^- ions.

PDPF-ASU-2.4 could not be dissolved in DMSO-d_6 and analyzed after immersion in 10 M aq. NaOH for 168 h at 90 °C, due to crosslinking generated by amino alcoholates.

To conclude, tethering piperidine-based cations via a methylene bridge instead of a heptyl chain showed improved OH^- conductivity and outstanding thermal and alkaline stability. Introducing the alicyclic piperidine-based cationic group via a methyl bridge to the polymer backbone can be considered a new and efficient strategy to improve the properties of AEMs.

Conclusion and future work

This thesis discusses different design strategies which can be used to improve the properties of AEMs. A variety of synthetic strategies have been employed to synthesize monomers. Superacid-mediated polyhydroxylalkylation and ATRP reactions were used to produce different polymer backbone architectures, which were then functionalized with QA groups. AEMs were cast and characterized with regard to hydroxide conductivity, water uptake, thermal and alkaline stability to elucidate the relationship between the polymer structure and properties.

Fluorene-based monomers were used to synthesize ether-free backbone architectures and to introduce different QA groups. The different polymers produced membranes with high thermal and alkaline stability and high OH^- conductivity. The ether-free fluorene-based polymer backbones only started to degrade above 350 °C and showed an outstanding alkaline stability with no degradation even after immersed in 2 M aq. NaOH at 120 °C for 168 h. Moreover, the high stiffness of the hydrophobic polymer reduced the water uptake. The hydroxide conductivities of the AEMs were high and were directly affected by the polymer architecture, thecationic groups, and how the latter were incorporated into the polymeric structure. Introducing the cationic group via flexible alkyl spacers and increasing the local cationic concentration were essential strategies that improve the membranes' OH^- conductivity and alkaline stability. In addition, the design and synthesis of the BAB triblock copolymers (BAB) of polyfluorene alkylene midblock densely tethered with cations flanked by hydrophobic polystyrene block improved the mechanical properties, the OH^- conductivity, and the alkaline stability of the membranes.

Regarding the choice of the cation, AEMs in this thesis were almost exclusively functionalized with mono- and spirocylic QA cations since they showed high alkaline stability and high OH^- conductivity. Alkyl spacer chains, enhancing the alkaline stability of the cationic group, were used to tether the cationic groups to the backbone. Dual piperidinium groups (bisPip) were used to increase the local ionic concentration and to facilitate the ion transport. In addition, to enhance the alkaline stability of the cationic groups, the DMP and ASU were preferably attached in the 4-positions. This strategy provided AEMs with enhanced alkaline stability.

Future work on these AEMs includes investigating their performance in water electrolyzers and fuel cell applications. The encouraging results obtained with AEMs in the present work motivate further investigations and development of AEMs based on fluorene. AEMs with different polymer architectures, including hyperbranched and grafted copolymers, could be synthesized to further improve the mechanical and thermochemical properties of the AEMs.

Popular Science Summary

Climate change, which is triggered by greenhouse gases produced from the consumption of fossil fuels for power generation, is considered one of the most serious global issues nowadays. An article published by Geilen in the Energy Strategy Reviews in 2019 emphasized the Paris agreement from (2015), which has the goal of restricting global warming to below 2 °C and neutralizing the climate worldwide by the middle of the 21st century. This means that the global energy required by 2050 should not exceed the global energy of 2015, and 60 % of it should be from renewable sources. Therefore, to accomplish this goal, many countries, companies, and research laboratories have focused on alternative renewable and sustainable energy sources such as hydro- and wind power, solar panel, as well as fuel cell for generating environmentally friendly power. Fuel cell technology can be applied both in stationary and automotive applications. Fuel cells is an advanced technology, which converts the chemical energy into electricity forming only water as a product. The development of this technology is focused on two essential components, that are the electrolyte and catalyst, since both play an important role, not only in the fuel cell performance and durability, but also in the final cost of the fuel cell. The electrolyte is solid polymeric membrane responsible for both the separation of the two electrodes (anode and cathode) and the transportation of ions from one electrode to the other during fuel cell operation. Based on the ion they transport, the membranes are divided into proton exchange membranes (PEMs) and anion exchange membranes (AEMs). This thesis work is dedicated to the design, synthesis, and investigation of AEMs, which can be applied to this environmentally friendly technology. The properties of the AEMs have a direct influence on the efficiency and long-term operation of the fuel cell. Due to the alkaline environment, requirements such as high conductivity and long-lasting chemical stability have been central challenges for this type of membrane.

In this thesis, different strategies have been applied to design and synthesize novel membranes to improve the chemical stability and ion conductivity of the AEM. Typically, the polymer backbone of the membranes is synthesized via different polymerization techniques and is subsequently functionalized with mono- and spirocyclic quaternary ammonium groups, respectively. The polymer backbone of the membranes is hydrophobic in nature and responsible for mechanical and physical properties, and the cationic group has a hydrophilic character and gives rise

to ion conductivity of the counter ion. The architecture of the polymer backbone, the structure of the cationic functional groups, as well as the way in which the cationic functional groups are incorporated into the polymer backbone, are varied to investigate the influence on the thermal and chemical stability, water uptake, and conductivities.

References

1. G. Merle, M. Wessling and K. Nijmeijer, *J Membrane Sci*, 2011, **377**, 1-35.
2. G. Wand, *Johnson Matthey plc*, 2006, **14**.
3. W. R. Grove, *The London, Edinburgh, and Dublin Philosophical Magazine and Journal of Science*, 1839, **14**, 127-130.
4. W. R. Grove, *The London, Edinburgh, and Dublin Philosophical Magazine and Journal of Science*, 1839, **15**, 287-293.
5. Y. Wang, K. S. Chen, J. Mishler, S. C. Cho and X. C. Adroher, *Applied energy*, 2011, **88**, 981-1007.
6. J. Larminie, A. Dicks and M. S. McDonald, *Fuel cell systems explained*, J. Wiley Chichester, UK, 2003.
7. M. Hannan, M. M. Hoque, A. Mohamed and A. Ayob, *Renewable and Sustainable Energy Reviews*, 2017, **69**, 771-789.
8. N. Li, M. D. Guiver and W. H. Binder, *Chemsuschem*, 2013, **6**, 1376-1383.
9. G. Couture, A. Alaaeddine, F. Boschet and B. Ameduri, *Prog Polym Sci*, 2011, **36**, 1521-1557.
10. K.-D. Kreuer, in *Fuel Cells*, Springer, 2013, pp. 1-7.
11. S. Zaidi, 2010.
12. E. Gülzow, *Fuel Cells*, 2004, **4**, 251-255.
13. M. R. Hibbs, C. H. Fujimoto and C. J. Cornelius, *Macromolecules*, 2009, **42**, 8316-8321.
14. Y. Chida, Y. Horiuchi, K. Kuroda and H. Yoshioka, *Nenryo Denchi*, 2010, **9**, 11-17.
15. S. McPhail, E. Simonetti, A. Moreno and R. Bove, in *Materials for Fuel Cells*, ed. M. Gasik, Woodhead Publishing, 2008, DOI: https://doi.org/10.1533/9781845694838.248, pp. 248-279.
16. C. Sun, R. Hui and J. Roller, *Journal of Solid State Electrochemistry*, 2010, **14**, 1125-1144.
17. M. Winter and R. J. Brodd, *Chem Rev*, 2004, **104**, 4245-4270.
18. Z. P. Cano, D. Banham, S. Ye, A. Hintennach, J. Lu, M. Fowler and Z. Chen, *Nat Energy*, 2018, **3**, 279-289.
19. A. Kirubakaran, S. Jain and R. Nema, *Renewable and sustainable energy reviews*, 2009, **13**, 2430-2440.
20. K. Jiao, J. Xuan, Q. Du, Z. Bao, B. Xie, B. Wang, Y. Zhao, L. Fan, H. Wang, Z. Hou, S. Huo, N. P. Brandon, Y. Yin and M. D. Guiver, *Nature*, 2021, **595**, 361-369.

21. D. Li, A. R. Motz, C. Bae, C. Fujimoto, G. Yang, F.-Y. Zhang, K. E. Ayers and Y. S. Kim, *Energ Environ Sci*, 2021, **14**, 3393-3419.
22. J.-H. Wee, *Renewable and Sustainable Energy Reviews*, 2007, **11**, 1720-1738.
23. J. R. Varcoe, P. Atanassov, D. R. Dekel, A. M. Herring, M. A. Hickner, P. A. Kohl, A. R. Kucernak, W. E. Mustain, K. Nijmeijer, K. Scott, T. W. Xu and L. Zhuang, *Energ Environ Sci*, 2014, **7**, 3135-3191.
24. M. Steilen and L. Jörissen, 2015.
25. A. Kusoglu and A. Z. Weber, *Chem Rev*, 2017, **117**, 987-1104.
26. A. Kraytsberg and Y. Ein-Eli, *Energy & Fuels*, 2014, **28**, 7303-7330.
27. M. A. Hickner, A. M. Herring and E. B. Coughlin, *Journal of Polymer Science Part B: Polymer Physics*, 2013, **51**, 1727-1735.
28. M. Mandal, G. Huang, N. Ul Hassan, W. E. Mustain and P. A. Kohl, *J Mater Chem A*, 2020, **8**, 17568-17578.
29. S. Hong, M. Hou, H. Zhang, Y. Jiang, Z. Shao and B. Yi, *Electrochimica Acta*, 2017, **245**, 403-409.
30. L. Duclos, M. Lupsea, G. Mandil, L. Svecova, P.-X. Thivel and V. Laforest, *Journal of Cleaner Production*, 2017, **142**, 2618-2628.
31. E. Gülzow, *J Power Sources*, 1996, **61**, 99-104.
32. J. R. Varcoe and R. C. Slade, *Fuel Cells*, 2005, **5**, 187-200.
33. E. Gülzow, *J Power Sources*, 1996, **61**, 99-104.
34. E. Gülzow and M. Schulze, *J Power Sources*, 2004, **127**, 243-251.
35. S. D. Poynton, J. P. Kizewski, R. C. T. Slade and J. R. Varcoe, *Solid State Ionics*, 2010, **181**, 219-222.
36. Z. Tao, C. Wang, X. Zhao, J. Li and M. D. Guiver, *Advanced Materials Technologies*, 2021, **6**, 2001220.
37. H. Chen, R. Tao, K.-T. Bang, M. Shao and Y. Kim, *Adv Energy Mater*, 2022, **12**, 2200934.
38. J. R. Varcoe, R. C. T. Slade and E. Lam How Yee, *Chemical Communications*, 2006, DOI: 10.1039/B600838K, 1428-1429.
39. H. A. Miller, K. Bouzek, J. Hnat, S. Loos, C. I. Bernaecker, T. Weissgarber, L. Rontzsch and J. Meier-Haack, *Sustain Energ Fuels*, 2020, **4**, 2114-2133.
40. W. E. Mustain, M. Chatenet, M. Page and Y. S. Kim, *Energ Environ Sci*, 2020, **13**, 2805-2838.
41. W. You, K. J. T. Noonan and G. W. Coates, *Prog Polym Sci*, 2020, **100**, 101177.
42. W. You, K. M. Hugar, R. C. Selhorst, M. Treichel, C. R. Peltier, K. J. T. Noonan and G. W. Coates, *The Journal of Organic Chemistry*, 2021, **86**, 254-263.
43. N. Chen and Y. M. Lee, *Trends in Chemistry*, 2022, **4**, 236-249.
44. J. Xue, J. Zhang, X. Liu, T. Huang, H. Jiang, Y. Yin, Y. Qin and M. D. Guiver, *Electrochemical Energy Reviews*, 2022, **5**, 348-400.
45. D. R. Dekel, *J Power Sources*, 2018, **375**, 158-169.
46. C. G. Arges and L. Zhang, *ACS Appl Energ Mater*, 2018, **1**, 2991-3012.

47. J. Ponce-González, D. K. Whelligan, L. Wang, R. Bance-Soualhi, Y. Wang, Y. Peng, H. Peng, D. C. Apperley, H. N. Sarode, T. P. Pandey, A. G. Divekar, S. Seifert, A. M. Herring, L. Zhuang and J. R. Varcoe, *Energ Environ Sci*, 2016, **9**, 3724-3735.
48. S. Maurya, S. Noh, I. Matanovic, E. J. Park, C. N. Villarrubia, U. Martinez, J. Han, C. Bae and Y. S. Kim, *Energ Environ Sci*, 2018, **11**, 3283-3291.
49. Y. J. Wang, J. L. Qiao, R. Baker and J. J. Zhang, *Chem Soc Rev*, 2013, **42**, 5768-5787.
50. M. A. Hickner, A. M. Herring and E. B. Coughlin, *J Polym Sci Pol Phys*, 2013, **51**, 1727-1735.
51. W. H. Lee, Y. S. Kim and C. Bae, *Acs Macro Lett*, 2015, **4**, 814-818.
52. W. H. Lee, A. D. Mohanty and C. Bae, *Acs Macro Lett*, 2015, **4**, 453-457.
53. K. F. L. Hagesteijn, S. X. Jiang and B. P. Ladewig, *J Mater Sci*, 2018, **53**, 11131-11150.
54. E. J. Park and Y. S. Kim, *J Mater Chem A*, 2018, **6**, 15456-15477.
55. N. Chen, Y. Jin, H. Liu, C. Hu, B. Wu, S. Xu, H. Li, J. Fan and Y. M. Lee, *Angewandte Chemie International Edition*, 2021, **60**, 19272-19280.
56. P. Jannasch and E. A. Weiber, *Macromol Chem Phys*, 2016, **217**, 1108-1118.
57. D. Pan, P. M. Bakvand, T. H. Pham and P. Jannasch, *J Mater Chem A*, 2022, **10**, 16478-16489.
58. S. Gu, R. Cai and Y. Yan, *Chemical Communications*, 2011, **47**, 2856-2858.
59. D. Pan, T. H. Pham and P. Jannasch, *ACS Appl Energ Mater*, 2021, **4**, 11652-11665.
60. G. W. He, Z. Li, J. Zhao, S. F. Wang, H. Wu, M. D. Guiver and Z. Y. Jiang, *Adv Mater*, 2015, **27**, 5280-5295.
61. N. Chen and Y. M. Lee, *Prog Polym Sci*, 2021, **113**.
62. M. G. Marino, J. P. Melchior, A. Wohlfarth and K. D. Kreuer, *J Membrane Sci*, 2014, **464**, 61-71.
63. D. Marx, A. Chandra and M. E. Tuckerman, *Chem Rev*, 2010, **110**, 2174-2216.
64. T. Zelovich, L. Vogt-Maranto, M. A. Hickner, S. J. Paddison, C. Bae, D. R. Dekel and M. E. Tuckerman, *Chem Mater*, 2019, **31**, 5778-5787.
65. M. R. Hibbs, M. A. Hickner, T. M. Alam, S. K. McIntyre, C. H. Fujimoto and C. J. Cornelius, *Chem Mater*, 2008, **20**, 2566-2573.
66. M. E. Tuckerman, D. Marx and M. Parrinello, *Nature*, 2002, **417**, 925-929.
67. D. Marx, *ChemPhysChem*, 2006, **7**, 1848-1870.
68. N. Li, T. Yan, Z. Li, T. Thurn-Albrecht and W. H. Binder, *Energ Environ Sci*, 2012, **5**, 7888-7892.
69. H. S. Dang, E. A. Weiber and P. Jannasch, *J Mater Chem A*, 2015, **3**, 5280-5284.
70. J. Ran, L. Wu, B. Wei, Y. Chen and T. Xu, *Sci Rep-Uk*, 2014, **4**, 6486.
71. J. R. Varcoe, R. C. Slade, E. Lam How Yee, S. D. Poynton, D. J. Driscoll and D. C. Apperley, *Chem Mater*, 2007, **19**, 2686-2693.
72. A. H. N. Rao, R. L. Thankamony, H. J. Kim, S. Nam and T. H. Kim, *Polymer*, 2013, **54**, 111-119.

73. J. Pan, C. Chen, Y. Li, L. Wang, L. Tan, G. Li, X. Tang, L. Xiao, J. Lu and L. Zhuang, *Energ Environ Sci*, 2014, **7**, 354-360.
74. H. S. Dang and P. Jannasch, *J Mater Chem A*, 2016, **4**, 11924-11938.
75. H.-S. Dang and P. Jannasch, *J Mater Chem A*, 2016, **4**, 17138-17153.
76. J. O. M. Bockris, *Int J Hydrogen Energ*, 2013, **38**, 2579-2588.
77. H. Zhang and P. K. Shen, *Chem Rev*, 2012, **112**, 2780-2832.
78. L. Wang, X. Peng, W. E. Mustain and J. R. Varcoe, *Energ Environ Sci*, 2019, **12**, 1575-1579.
79. E. J. Park, S. Maurya, M. R. Hibbs, C. H. Fujimoto, K.-D. Kreuer and Y. S. Kim, *Macromolecules*, 2019, **52**, 5419-5428.
80. N. Chen, C. Hu, H. H. Wang, S. P. Kim, H. M. Kim, W. H. Lee, J. Y. Bae, J. H. Park and Y. M. Lee, *Angewandte Chemie International Edition*, 2021, **60**, 7710-7718.
81. A. D. Mohanty and C. Bae, *J Mater Chem A*, 2014, **2**, 17314-17320.
82. N. Chen, J. H. Park, C. Hu, H. H. Wang, H. M. Kim, N. Y. Kang and Y. M. Lee, *J Mater Chem A*, 2022, **10**, 3678-3687.
83. H. H. Wang, C. Hu, J. H. Park, H. M. Kim, N. Y. Kang, J. Y. Bae, W. H. Lee, N. Chen and Y. M. Lee, *J Membrane Sci*, 2022, **644**, 120160.
84. C. G. Arges and V. Ramani, *P Natl Acad Sci USA*, 2013, **110**, 2490-2495.
85. M. G. Marino and K. D. Kreuer, *Chemsuschem*, 2015, **8**, 513-523.
86. T. J. Peckham and S. Holdcroft, *Adv Mater*, 2010, **22**, 4667-4690.
87. O. D. Thomas, K. J. W. Y. Soo, T. J. Peckham, M. P. Kulkarni and S. Holdcroft, *J Am Chem Soc*, 2012, **134**, 10753-10756.
88. H. Long and B. Pivovar, *The Journal of Physical Chemistry C*, 2014, **118**, 9880-9888.
89. F. Gu, H. Dong, Y. Li, Z. Si and F. Yan, *Macromolecules*, 2014, **47**, 208-216.
90. K. M. Hugar, H. A. Kostalik IV and G. W. Coates, *J Am Chem Soc*, 2015, **137**, 8730-8737.
91. J. T. Fan, A. G. Wright, B. Britton, T. Weissbach, T. J. G. Skalski, J. Ward, T. J. Peckham and S. Holdcroft, *Acs Macro Lett*, 2017, **6**, 1089-1093.
92. J. Fan, A. G. Wright, B. Britton, T. Weissbach, T. J. Skalski, J. Ward, T. J. Peckham and S. Holdcroft, *Acs Macro Lett*, 2017, **6**, 1089-1093.
93. J. T. Fan, S. Willdorf-Cohen, E. M. Schibli, Z. Paula, W. Li, T. J. G. Skalski, A. T. Sergeenko, A. Hohenadel, B. J. Frisken, E. Magliocca, W. E. Mustain, C. E. Diesendruck, D. R. Dekel and S. Holdcroft, *Nat Commun*, 2019, **10**.
94. W. Zhang, Y. Liu, A. C. Jackson, A. M. Savage, S. P. Ertem, T.-H. Tsai, S. Seifert, F. L. Beyer, M. W. Liberatore and A. M. Herring, *Macromolecules*, 2016, **49**, 4714-4722.
95. B. Zhang, H. Long, R. B. Kaspar, J. Wang, S. Gu, Z. Zhuang, B. Pivovar and Y. Yan, *Rsc Adv*, 2018, **8**, 26640-26645.
96. B. Zhang, R. B. Kaspar, S. Gu, J. Wang, Z. Zhuang and Y. Yan, *Chemsuschem*, 2016, **9**, 2374-2379.

97. A. M. Ahmed Mahmoud and K. Miyatake, *J Membrane Sci*, 2022, **643**, 120072.
98. M. R. Hibbs, *Journal of Polymer Science Part B: Polymer Physics*, 2013, **51**, 1736-1742.
99. Z. Zhang, L. Wu, J. Varcoe, C. Li, A. L. Ong, S. Poynton and T. Xu, *J Mater Chem A*, 2013, **1**, 2595-2601.
100. J.-S. Park, S.-H. Park, S.-D. Yim, Y.-G. Yoon, W.-Y. Lee and C.-S. Kim, *J Power Sources*, 2008, **178**, 620-626.
101. F. Zhang, T. Li, W. Chen, X. Wu, X. Yan, W. Xiao, Y. Zhang, X. Wang and G. He, *Acs Appl Mater Inter*, 2021, **13**, 10490-10499.
102. A. D. Mohanty, S. E. Tignor, J. A. Krause, Y.-K. Choe and C. Bae, *Macromolecules*, 2016, **49**, 3361-3372.
103. X. Wang, W. B. Sheng, Y. H. Shen, L. Liu, S. Dai and N. W. Li, *J Membrane Sci*, 2019, **587**.
104. T. Jiang, C. Wu, Y. Zhou, S. Cheng, S. Yang, H. Wei, Y. Ding and Y. Wu, *J Membrane Sci*, 2022, **647**, 120342.
105. Y. S. Kim, *ACS Applied Polymer Materials*, 2021, **3**, 1250-1270.
106. H. Ono, J. Miyake, S. Shimada, M. Uchida and K. Miyatake, *J Mater Chem A*, 2015, **3**, 21779-21788.
107. A. M. A. Mahmoud, A. M. M. Elsaghier, K. Otsuji and K. Miyatake, *Macromolecules*, 2017, **50**, 4256-4266.
108. A. G. Wright, T. Weissbach and S. Holdcroft, *Angew Chem Int Edit*, 2016, **55**, 4818-4821.
109. M. G. Zolotukhin, S. Fomine, L. M. Lazo, M. D. C. G. Hernández, M. T. Guzmán-Gutiérrez, A. Ruiz-Trevino, D. Fritsch, D. C. Cuellas and J. M. Fernandez-G, *High Performance Polymers*, 2007, **19**, 638-648.
110. W. H. Lee, E. J. Park, J. Han, D. W. Shin, Y. S. Kim and C. Bae, *Acs Macro Lett*, 2017, **6**, 566-570.
111. J. S. Olsson, T. H. Pham and P. Jannasch, *Adv Funct Mater*, 2018, **28**.
112. A. Allushi, T. H. Pham and P. Jannasch, *J Membrane Sci*, 2021, **632**, 119376.
113. A. Allushi, T. H. Pham, J. S. Olsson and P. Jannasch, *J Mater Chem A*, 2019, **7**, 27164-27174.
114. T. H. Pham, J. S. Olsson and P. Jannasch, *J Mater Chem A*, 2018, **6**, 16537-16547.
115. J. S. Olsson, T. H. Pham and P. Jannasch, *Macromolecules*, 2020, **53**, 4722-4732.
116. T. H. Pham, A. Allushi, J. S. Olsson and P. Jannasch, *Polym Chem-Uk*, 2020, **11**, 6953-6963.
117. H. S. Dang and P. Jannasch, *J Mater Chem A*, 2017, **5**, 21965-21978.
118. A. D. Mohanty, C. Y. Ryu, Y. S. Kim and C. Bae, *Macromolecules*, 2015, **48**, 7085-7095.
119. G. Saikia and P. K. Iyer, *The Journal of Organic Chemistry*, 2010, **75**, 2714-2717.
120. S. H. Oh, S. I. Na, Y. C. Nah, D. Vak, S. S. Kim and D. Y. Kim, *Org Electron*, 2007, **8**, 773-783.

121. S. Kotha, K. Lahiri and D. Kashinath, *Tetrahedron*, 2002, **58**, 9633-9695.
122. C. C. C. Johansson Seechurn, M. O. Kitching, T. J. Colacot and V. Snieckus, *Angewandte Chemie International Edition*, 2012, **51**, 5062-5085.
123. G. A. Molander and N. Ellis, *Accounts Chem Res*, 2007, **40**, 275-286.
124. A. L. Casado and P. Espinet, *Organometallics*, 1998, **17**, 954-959.
125. J. Zhou and G. C. Fu, *J Am Chem Soc*, 2004, **126**, 1340-1341.
126. B. Saito and G. C. Fu, *J Am Chem Soc*, 2007, **129**, 9602-9603.
127. J. H. Kirchhoff, M. R. Netherton, I. D. Hills and G. C. Fu, *J Am Chem Soc*, 2002, **124**, 13662-13663.
128. L. I. Olvera, M. T. Guzmán-Gutiérrez, M. G. Zolotukhin, S. Fomine, J. Cárdenas, F. A. Ruiz-Trevino, D. Villers, T. A. Ezquerra and E. Prokhorov, *Macromolecules*, 2013, **46**, 7245-7256.
129. E. R. Peña, M. Zolotukhin and S. Fomine, *Macromolecules*, 2004, **37**, 6227-6235.
130. M. T. Guzmán-Gutiérrez, D. R. Nieto, S. Fomine, S. L. Morales, M. G. Zolotukhin, M. C. G. Hernandez, H. Kricheldorf and E. S. Wilks, *Macromolecules*, 2011, **44**, 194-202.
131. D. A. Klumpp, *ARKIVOC: Online Journal of Organic Chemistry*, 2009.
132. M. J. O'Connor, K. N. Boblak, A. D. Spitzer, P. A. Gucciardo, A. M. Baumann, J. W. Peter, C. Y. Chen, R. Peter, A. A. Mitton and D. A. Klumpp, *Tetrahedron Letters*, 2010, **51**, 4984-4987.
133. A. R. Cruz, M. C. G. Hernandez, M. T. Guzmán-Gutiérrez, M. G. Zolotukhin, S. Fomine, S. L. Morales, H. Kricheldorf, E. S. Wilks, J. Cárdenas and M. Salmón, *Macromolecules*, 2012, **45**, 6774-6780.
134. E. R. Peña, M. Zolotukhin and S. Fomine, *Polymer*, 2005, **46**, 7494-7503.
135. H. Odian, *Principle of polymerization*, 2001.
136. J.-S. Wang and K. Matyjaszewski, *J Am Chem Soc*, 1995, **117**, 5614-5615.
137. K. Matyjaszewski and J. Xia, *Chem Rev*, 2001, **101**, 2921-2990.
138. K. Matyjaszewski, *Macromolecules*, 2012, **45**, 4015-4039.
139. H. Nederstedt, Lund University, 2021.
140. W. Tang and K. Matyjaszewski, *Macromolecules*, 2006, **39**, 4953-4959.
141. W. Tang and K. Matyjaszewski, *Macromolecules*, 2007, **40**, 1858-1863.
142. J. Gao, *J Am Chem Soc*, 1991, **113**, 7796-7797.
143. T. H. Pham, J. S. Olsson and P. Jannasch, *J Mater Chem A*, 2019, **7**, 15895-15906.
144. A. G. Kikhney and D. I. Svergun, *FEBS Letters*, 2015, **589**, 2570-2577.
145. B. R. Pauw, *Journal of Physics: Condensed Matter*, 2013, **25**, 383201.
146. N. A. Geisse, *Materials Today*, 2009, **12**, 40-45.
147. L. Gross, F. Mohn, N. Moll, P. Liljeroth and G. Meyer, *Science*, 2009, **325**, 1110-1114.
148. H. S. Magar, R. Y. A. Hassan and A. Mulchandani, *Sensors (Basel, Switzerland)*, 2021, **21**.

Printed by Media-Tryck, Lund 2022 NORDIC SWAN ECOLABEL 3041 0903

ISBN 978-91-7422-902-8

Centre for Analysis and Synthesis
Department of Chemistry
Faculty of Engineering
Lund University

LUND UNIVERSITY